

# Targeting SARS-CoV-2 Receptor Binding Domain with Stapled Peptides: An *In Silico* Study

Luana Janaína de Campos, Nicholas Y. Palermo, and Martin Conda-Sheridan\*

Cite This: *J. Phys. Chem. B* 2021, 125, 6572–6586

Read Online

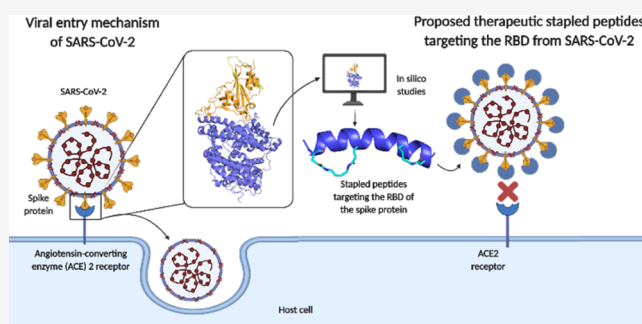
ACCESS |

Metrics & More

Article Recommendations

Supporting Information

**ABSTRACT:** Severe acute respiratory syndrome coronavirus 2 (SARS-CoV-2) has evolved into a pandemic of unprecedented scale. This coronavirus enters cells by the interaction of the receptor binding domain (RBD) with the human angiotensin-converting enzyme 2 receptor (hACE2). In this study, we employed a rational structure-based design to propose 22-mer stapled peptides using the structure of the hACE2  $\alpha$ 1 helix as a template. These peptides were designed to retain the  $\alpha$ -helical character of the natural structure, to enhance binding affinity, and to display a better solubility profile compared to other designed peptides available in the literature. We employed different docking strategies (PATCHDOCK and ZDOCK) followed by a double-step refinement process (FIBERDOCK) to rank our peptides, followed by stability analysis/evaluation of the interaction profile of the best docking predictions using a 500 ns molecular dynamics (MD) simulation, and a further binding affinity analysis by molecular mechanics with generalized Born and surface area (MM/GBSA) method. Our most promising stapled peptides presented a stable profile and could retain important interactions with the RBD in the presence of the E484K RBD mutation. We predict that these peptides can bind to the viral RBD with similar potency to the control NYBSP-4 (a 30-mer experimentally proven peptide inhibitor). Furthermore, our study provides valuable information for the rational design of double-stapled peptide as inhibitors of SARS-CoV-2 infection.



## 1. INTRODUCTION

During December 2019, several cases of pneumonia, resulting from an unknown virus, were reported in Wuhan, the capital of Hubei province in China. Later, it was determined the illness was caused by a novel coronavirus, which was named severe acute respiratory syndrome coronavirus 2 (SARS-CoV-2).<sup>1</sup> Unfortunately, the disease evolved into a pandemic of monumental proportions<sup>2</sup> that has resulted in more than 162 million reported cases and over 3.3 million deaths around the world by May 2021 according to the World Health Organization (WHO).<sup>3</sup> The deleterious consequences of this pandemic have made COVID-19 an economic, social, and public health crisis.<sup>4–6</sup> Although some vaccines have reached the market, additional interventions are needed in the following scenarios: (1) vaccine efficacy could be affected by new viral mutations or improper storage; (2) patients not able to receive a vaccine due to health challenges or unavailability; or (3) a segment of the population averse to receiving vaccinations.

The coronaviruses (COVs) are enveloped, single-stranded RNA viruses that cause severe respiratory complications.<sup>7</sup> Some SARS-CoV-2 features include its rapid spread, ease of contagion, and a death toll of 3% of the diagnosed cases.<sup>2</sup> The SARS-CoV-2 virion is composed of four proteins: a spike protein (S), a membrane glycoprotein (M), an envelope

protein (E), and a nucleocapsid protein (N).<sup>8,9</sup> The spike protein, which is found at the virus surface, is widely accepted as the key player in the infection process.<sup>2,10,11</sup> This protein can be divided into distinct areas: a receptor binding domain (RBD), a central helix/heptad repeat, and a C-terminal region that associates with the plasma membrane of human cells.<sup>12,13</sup> The RBD of the S protein undergoes conformational changes to maximize its association with its target, the human angiotensin-converting enzyme 2 (hACE2), to achieve human contagion.<sup>9,14,15</sup> Thereafter, host proteases cleave the S protein into two subdomains: an N-terminal S1 portion and a membrane-bound C-terminal S2 unit. The receptor binding event and the proteolytic cleavage work synergistically to promote viral entry into human cells.<sup>10</sup> It has been reported that the SARS-CoV-2 RBD presents 10–20 times higher binding affinity for hACE2 ( $\sim$ 15 nM) than the RBD of SARS-CoV.<sup>13,16,17</sup> A recent *in silico* study conducted by Ponga and

Received: March 16, 2021

Revised: May 26, 2021

Published: June 11, 2021



co-workers<sup>18</sup> evaluated the binding affinity and bond-breaking force between the SARS-CoV-2 spike protein and hACE2 receptors. The model estimated an energy of  $12.6 \pm 1$  kcal/mol, resulting in a dissociation constant of  $K_D = 1.3$  nM, highlighting the high affinity of the complex.

Given its role in infection, affecting the interaction between the S protein RBD and the hACE2 has been identified as a promising strategy to prevent SARS-CoV-2 contagion.<sup>2,19–24</sup> Crystal structures of the S protein and the hACE2 show that the RBD presents a network of H-bonds with the  $\alpha 1$  and  $\alpha 2$  helices and a loop linking the  $\beta 3$  and  $\beta 4$  antiparallel strands on the hACE2 protein.<sup>17,21,25</sup> However, most of the key interactions are between the RBD of the S protein and the  $\alpha 1$  helix.<sup>7,26</sup>

The first potential peptide therapeutic against SARS-CoV-2, to our knowledge, was reported by the Pentelute group.<sup>27</sup> These scientists designed 23-mer peptides derived from the hACE2  $\alpha 1$  domain, which were refined by molecular dynamics (MD) simulations. Bio-layer interferometry on the top designed peptide showed that the structure presented a dissociation constant,  $K_D$ , of  $1.3 \mu\text{M}$  for the Sino Biological insect-derived SARS-CoV-2-RBD (the binding of the 23-mer sequence derived from the hACE2 was not reported), a value around 100 times higher compared to the results published by Wrapp et al. for the binding of the hACE2 full length and the spike protein, which determined a  $K_D$  of  $\sim 14.7$  nM.<sup>13</sup> Nevertheless, this was the first precedent to demonstrate that peptides could be used as therapeutics against SARS-CoV-2. Unfortunately, the N-termini biotinylated peptide from the Pentelute group<sup>27</sup> did not associate with human embryonic kidney (HEK) expressing the SARS-CoV-2-RBD or other insect-derived variants. In a theoretical study, Basit and co-workers designed a truncated hACE2 peptide that was 98 amino acids long. *In silico* studies using ZDOCK followed by MD simulations predicted the designed peptide should bind to the S protein RBD with higher affinity than the native hACE2 protein ( $\Delta G$  of  $-12.7$  and  $-10.7$  kcal/mol, respectively).<sup>28</sup> The group of Rana performed MD simulations of 136 different 23-mer peptides.<sup>29</sup> The researchers suggested that their top peptide should present higher affinity for the RBD domain than the native hACE2 peptide as can be deduced by the obtained binding free energies:  $-304.1$  vs  $-155.8$  kJ/mol, respectively. Another intriguing study was done by Sithiyotha and Chunsriviro.<sup>30</sup> These authors cleverly combined computational protein design (Rosetta) and MD simulations (AMBER) to generate a library of 25-mer peptides based on residues 21–45 of the  $\alpha 1$  helix of hACE2. Their results predict that their peptides will display higher affinity toward the SARS-CoV-2-RBD than the peptides developed by the Pentelute group.<sup>23</sup> Another study that is noteworthy was reported by Chowdhury and co-workers.<sup>31</sup> In such study, the authors used docking to screen 50 peptides that presented known activity against SARS-CoV-1 and, after MD simulation analysis, have identified two leads (29-mer and 33-mer peptides) that should inhibit SARS-CoV-2. A theoretical study done by Han and Král<sup>7</sup> showed that a peptide containing elements from the hACE2  $\alpha 1$  and  $\alpha 2$  helices (ca. 75–139 mer), with the addition of carefully selected linkers to stabilize the peptidic structure, presents more stability and better binding affinity to the RBD than a peptide derived only from the  $\alpha 1$  helix (34-mer).<sup>7</sup> For a complete review on bioactive peptides in the perspective of their potential activity against SARS-CoV-2, we recommend to

read the literature review conducted by Bhullar and co-workers.<sup>32</sup>

The work of Han and Král<sup>7</sup> identified the importance of  $\alpha$ -helix stability on therapeutic peptides against COVID-19, a key feature that can be appreciated on available crystal structures (Protein Data Bank (PDB): 6M0J, 6M17). The main consideration when designing this type of therapeutics is that short peptides could lose their secondary structure,<sup>33</sup> leading to a disruption of the bioactive conformation in the absence of a complete protein fold.<sup>34</sup> As a result, the therapeutic utility of such structures would be limited. Thus, a longer peptide would be desirable to keep the  $\alpha$ -helical character. However, it may be unpractical from an immunogenic, synthetic, and cost perspective to prepare long peptides. Shorter sequences ( $\sim 25$  mer) will be attractive therapeutics due to lower production costs and higher yield. However, such molecules should be able to maintain their secondary structure, be stable to degradation, and present good water solubility.

As can be appreciated from the discussion above, there are few studies exploring peptide-based antivirals to treat COVID-19. Herein, we designed short peptide sequences that may keep their 2<sup>nd</sup> structure and display high metabolic stability. Stapled peptides are a novel therapeutic modality that allows locking a structure in its bioactive conformation through the site-specific introduction of a chemical linker.<sup>34–36</sup> These peptides can inhibit intracellular protein–protein interactions (PPIs), such as in the case of SARS-CoV-2/hACE2, because they are capable of covering multiple contact points.<sup>34,37,38</sup> Further, the addition of a staple can keep the 2<sup>nd</sup> structure in place.<sup>36,39</sup> An additional advantage of such bonds is their higher metabolic stability due to their improved proteolytic resistance (compared to natural amino acids).<sup>34</sup>

Recently, while this work was in progress, Curreli and co-workers<sup>40</sup> reported the design, synthesis, and biological evaluation of 30-mer double-hydrocarbon stapled peptides based on the hACE2 helix (no computer simulation was associated to their work). The reported stapled peptides showed high helical contents (50–94% helicity), no cytotoxicity at the highest dose tested, a good profile of resistance to degradation by proteolytic enzymes in human plasma and the most active peptide possessed antiviral activity (half-maximal inhibitory concentration ( $IC_{50}$ ) reported around: 1.9–4.1 mM and 2.2–2.8 mM) measured in different cell lines. Maas et al. also reported the synthesis and evaluation of hACE2-derived 35-mer peptides containing a mono-lactam bridge that are able to inhibit the RBD–hACE2 complex formation.<sup>41</sup> Their lead peptide presented increased affinity for the RBD ( $IC_{50}$ : 3.6  $\mu\text{M}$ ,  $K_D$ : 2.1  $\mu\text{M}$ ) compared with the control group; a 35-mer sequence extracted from the hACE2. In contrast, Morgan et al. reported that their 23-mer mono-stapled peptides effectively constrained the helical structure in solution, but none of those peptides prevented virus internalization,<sup>42</sup> which indicates that must be an optimal peptide length and number/position of the staples to reach antiviral activity. Moreover, these results agree and validate our theory that using stapled peptides derived from the  $\alpha 1$  helix of hACE2 could lay the foundations for further optimization of a potential clinical candidate.

Therefore, since (to date) no SARS-CoV-2 specific drug has been described and the currently proposed pharmacological treatments are based on repurposed drugs,<sup>43,44</sup> aiming to develop novel therapeutics against SARS-CoV-2, we performed *in silico* studies of short, 22-mer stapled peptides that mimic

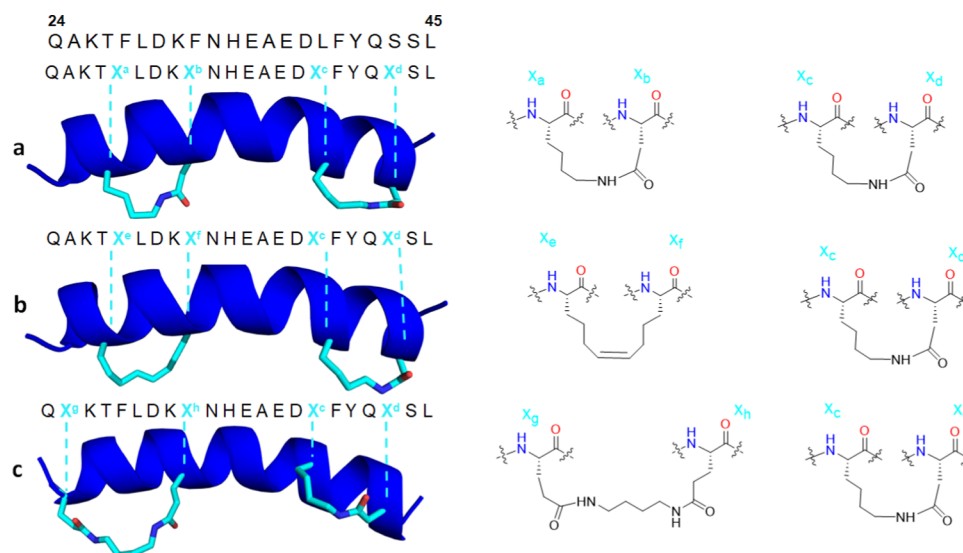


**Figure 1.** Template sequence and structural basis of the proposed stapled modifications. (a) Lactam bridge replacing residues Phe28 and Phe32 and Leu39 and Ser43; (b) alkene stapling brace replacing Phe28 and Phe32 and lactam bridge replacing Leu39 and Ser43; (c) double-lactam bridge between Ala25 and Phe32 and lactam bridge replacing Leu39 and Ser43. Left: three-dimensional (3D) model. Right: two-dimensional (2D) structures of the proposed stapled bonds. "X" denotes the position of the staple within each peptide.

**Table 1.** Description of the Sequence of the Proposed Stapled Peptides<sup>a</sup>

Designed stapled peptide	Sequence
22-mer hACE2 from $\alpha$ 1 helix	QAKTFLDKFNHEAEDLFYQSSL
Original 1	QAKT <sup>X<sup>a</sup></sup> LDK <sup>X<sup>b</sup></sup> NHEAED <sup>X<sup>c</sup></sup> FYQ <sup>X<sup>d</sup></sup> SL
Modification 1	QAKT <sup>X<sup>a</sup></sup> LEK <sup>X<sup>b</sup></sup> NHEAED <sup>X<sup>c</sup></sup> FYQ <sup>X<sup>d</sup></sup> SL
Modification 2	QAKT <sup>X<sup>a</sup></sup> LDK <sup>X<sup>b</sup></sup> NHEAED <sup>X<sup>c</sup></sup> FYQ <sup>X<sup>d</sup></sup> SQ
Modification 3	QAKT <sup>X<sup>a</sup></sup> LEK <sup>X<sup>b</sup></sup> NHEAED <sup>X<sup>c</sup></sup> FYQ <sup>X<sup>d</sup></sup> SQ
Modification 4	QAKT <sup>X<sup>a</sup></sup> DKX <sup>b</sup> NHEAED <sup>X<sup>c</sup></sup> FYQ <sup>X<sup>d</sup></sup> SK(Ac)
Modification 5	QAKT <sup>X<sup>a</sup></sup> LEK <sup>X<sup>b</sup></sup> NHEAED <sup>X<sup>c</sup></sup> FYQ <sup>X<sup>d</sup></sup> SK(Ac)
Original 2	QAKT <sup>X<sup>e</sup></sup> LDK <sup>X<sup>f</sup></sup> NHEAED <sup>X<sup>c</sup></sup> FYQ <sup>X<sup>d</sup></sup> SL
Modification 6	QAKT <sup>X<sup>e</sup></sup> LEK <sup>X<sup>f</sup></sup> NHEAED <sup>X<sup>c</sup></sup> FYQ <sup>X<sup>d</sup></sup> SL
Modification 7	QAKT <sup>X<sup>e</sup></sup> LDK <sup>X<sup>f</sup></sup> NHEAED <sup>X<sup>c</sup></sup> FYQ <sup>X<sup>d</sup></sup> SQ
Modification 8	QAKT <sup>X<sup>e</sup></sup> LEK <sup>X<sup>f</sup></sup> NHEAED <sup>X<sup>c</sup></sup> FYQ <sup>X<sup>d</sup></sup> SQ
Modification 9	QAKT <sup>X<sup>e</sup></sup> LDK <sup>X<sup>f</sup></sup> NHEAED <sup>X<sup>c</sup></sup> FYQ <sup>X<sup>d</sup></sup> SK(Ac)
Modification 10	QAKT <sup>X<sup>e</sup></sup> LEK <sup>X<sup>f</sup></sup> NHEAED <sup>X<sup>c</sup></sup> FYQ <sup>X<sup>d</sup></sup> SK(Ac)
Original 3	QAKT <sup>X<sup>g</sup></sup> LDK <sup>X<sup>h</sup></sup> NHEAED <sup>X<sup>c</sup></sup> FYQ <sup>X<sup>d</sup></sup> SL
Modification 11	QAKT <sup>X<sup>g</sup></sup> LEK <sup>X<sup>h</sup></sup> NHEAED <sup>X<sup>c</sup></sup> FYQ <sup>X<sup>d</sup></sup> SL
Modification 12	QAKT <sup>X<sup>g</sup></sup> LDK <sup>X<sup>h</sup></sup> NHEAED <sup>X<sup>c</sup></sup> FYQ <sup>X<sup>d</sup></sup> SQ
Modification 13	QAKT <sup>X<sup>g</sup></sup> LEK <sup>X<sup>h</sup></sup> NHEAED <sup>X<sup>c</sup></sup> FYQ <sup>X<sup>d</sup></sup> SQ
Modification 14	QAKT <sup>X<sup>g</sup></sup> LDK <sup>X<sup>h</sup></sup> NHEAED <sup>X<sup>c</sup></sup> FYQ <sup>X<sup>d</sup></sup> SK(Ac)
Modification 15	QAKT <sup>X<sup>g</sup></sup> LEK <sup>X<sup>h</sup></sup> NHEAED <sup>X<sup>c</sup></sup> FYQ <sup>X<sup>d</sup></sup> SK(Ac)

<sup>a</sup>The staples insertion positions are highlighted in blue (according to the description from Figure 1), and the replacement of original residues is highlighted in red.

the structure of the hACE2 receptor to identify candidates with higher affinity for the S protein RBD using different stapling chemical groups. We postulate such peptides will prevent the RBD–hACE2 association halting virus entry in human cells,<sup>7,23</sup> while displaying increased physicochemical and biological stabilities.

## 2. METHODS

**2.1. Peptide Design.** We analyzed the structure of the hACE2 protein and its interactions with the RBD of the SARS-

CoV-2 S protein to rationally design our inhibitors.<sup>17</sup> As indicated by Král<sup>7</sup> and Hazelhurst,<sup>26</sup> the  $\alpha$ 1 helix of hACE2 contains 10 out of 15 residues believed to be important for association with the RBD: Gln24, Tyr27, Asp30, Lys31, His34, Glu35, Glu37, Asp38, Tyr41, Gln42. Thus, our strategy focused on extracting a 22-mer peptide that maintains these relevant amino acids while including changes to improve  $\alpha$ -helical stability and to optimize interactions with the RBD. As mentioned, other important residues from the hACE2 protein were not considered to avoid the design of inhibitors with a



long peptide sequence, which will be unpractical from a synthetic point of view.

Others have suggested the  $\alpha$ -helical character is key for the interaction of hACE2 with the RBD.<sup>7</sup> Interestingly, around residue 37 there is a kink, or bend, within the peptide that gives the appearance of two connected  $\alpha$ -helices. This detail was considered during the design to allow the peptide to arrange in this bent conformation. Therefore, the proposed modifications to preserve the  $\alpha$ -helical structure were located before or after residue 37. In our design, we introduced changes considering two aspects: (i) modifications to lock the secondary structure to preserve the  $\alpha$ -helical conformation and to increase metabolic stability; and (ii) alterations to increase the affinity of the peptides for the RBD.

Regarding the first strategy, we introduced a lactam bridge by replacing residues Phe28 and Phe32 (Figure 1a, indicated by X<sup>a</sup> and X<sup>b</sup>). These two residues were chosen to achieve the optimal connection at residues  $i$  and  $i + 4$ ,<sup>45–47</sup> between the amide-forming amino acids. We hypothesize this change will not alter the interactions because the Phe residues do not face the S protein RBD but will lock the  $\alpha$ -helical conformation of the peptide.<sup>45–47</sup> Moreover, since two aromatic groups are removed, this will reduce the lipophilicity of the peptide (the calculated Log  $P$  of an FF dimer is 0.42, while the  $K_D$  lactam bridge is  $-1.68$ <sup>48</sup>). The same lactam bridge was proposed for the Leu39 and Ser43 residues (Figure 1a–c, indicated by X<sup>c</sup> and X<sup>d</sup>). In addition, we proposed stapled peptides replacing the same residues (Phe28 and Phe32) with alkenes (Figure 1b, indicated by X<sup>e</sup> and X<sup>f</sup>). In this design, the optimal distance for connection is also at residues  $i$  and  $i + 4$ .<sup>45,49</sup> We postulate these new bonds will increase metabolic stability; *i.e.*, stapled peptides will be more resistant to proteases (although they may be oxidized). Another proposed change included a double-lactam bridge between Ala25 and Phe32 using 1,4-diaminobutane (Figure 1c, indicated by X<sup>g</sup> and X<sup>h</sup>). One interesting characteristic about our designed peptides, compared to the ones proposed by Curreli et al.,<sup>40</sup> is the hydrophobic profile of the final structures. Our staples substitute hydrophobic residues in the original structure (*i.e.*, Ala25, Phe28, Phe32, and Leu39). These changes should reduce the hydrophobic character of the peptides and, consequently, might display enhanced solubility in aqueous media.

To further increase affinity for the S protein, we included amino acids that may form additional interactions with the RBD. For example, Asp30 was replaced by Glu to maximize contacts with Lys417 on the S protein. Additionally, for some proposed structures, the Leu45 on the C termini was substituted by an acetylated Lys [K(Ac)] or a Gln to maximize contacts with Gly446. This latter change should also enhance water solubility. The sequence of all design stapled peptides is presented in Table 1 and their 2D structures can be found in the Supporting Information (SI) (Figure S1). An interesting aspect of our peptides is the fact that they were designed based on a short domain of the hACE2  $\alpha$ 1 helix (Figure S2). Therefore, they are expected to be active against strains possessing mutations in the RBD that are distant from the interaction points found in the 22-mer hACE2  $\alpha$ 1 helix. Examples of such mutations are Asn439Lys<sup>50</sup> (N439K) and Leu452Arg (L452R). According to the Centers for Disease Control and Prevention (CDC), the last cited mutation is associated with reduced effectiveness of treatments based on monoclonal antibodies.<sup>51,52</sup>

**2.2. Preparation of Protein and Peptides.** The structure of the receptor and the peptides were obtained from the crystal structure of hACE2 bound to the RBD of SARS-CoV-2 (PDB: 6M0J).<sup>25</sup> For the docking protocol, the receptor employed was composed of the entire structure of the glycosylated RBD from SARS-CoV-2. The file was energy minimized using UCSF Chimera software version 1.14.<sup>53</sup> Amber ff14SB force field was used to assign charges to the structure and the parameters for the energy optimization were: steepest descent steps were set to 1000; steepest descent step size 0.02 Å; conjugate gradient steps 1000, conjugate gradient step size 0.02 Å. Then, DockPrep tool in UCSF Chimera software was employed to: remove water molecules, repair truncated side chains, add hydrogens, and assign partial charges. Protonation states were assigned at physiological pH ( $\sim$ 7.4). The structures of the peptides were built from the crystal structure using the 22 residues of the hACE2  $\alpha$ 1 helix that lie on the interface between RBD and hACE2: Gln24, Ala25, Lys26, Tyr27, Phe28, Leu29, Asp30, Lys31, Phe32, Asn33, His34, Glu35, Asp36, Glu37, Asp38, Leu39, Phe40, Tyr41, Gln42, Ser43, Ser44, Leu45. The 18 peptides were built from the hACE2 original structure minimized (to maintain its natural conformation). This sequence was altered according to the proposed modifications (see Figure S1 (SI) for more details regarding the structures of all of the proposed peptides) followed by structure energy minimization in all positions where modifications were assigned (as described before for the receptor). Additionally, for comparison purposes, the best hydrocarbon stapled peptide based on the hACE2 helix published by Curreli and co-workers,<sup>40</sup> peptide NYBSP-4, was also modeled using the same protocol employed with the designed peptides. The NYBSP-4 peptide was also docked and underwent MD simulations using the same approaches described below. Furthermore, after the analysis of our MD results, we decided to analyze how our best stapled peptide would behave in the presence of mutations in the RBD. Therefore, we utilized the same crystal structure (PDB: 6M0J) and modified it in UCSF Chimera using the Dunbrack backbone-dependent rotamer library<sup>54</sup> provided with this software (version 1.14).<sup>53</sup> The mutated RBD was submitted to MD simulation using the protocol described in the MD section

**2.3. Generation of Docking Solutions.** To predict the binding affinity of our proposed peptides to the SARS-CoV-2 RBD, we used a rigid body protein–protein docking approach employing two docking servers: ZDOCK web server<sup>55</sup> and PATCHDOCK web server.<sup>56</sup> ZDOCK uses a fast Fourier transform (FFT) algorithm to allow an efficient global docking search. The method searches for all possible binding modes in the translational and rotational space between the protein and peptide, evaluating each pose using an energy-based scoring function. The energy function used by ZDOCK is Z score, which is cumulative of pairwise shape complementarity function with desolvation and electrostatics. Finally, the ZDOCK method ranks the predicted docking poses based on the Z score generated for each solution.<sup>57</sup> PATCHDOCK employs an algorithm based on shape complementarity principles to obtain the docking solutions and uses PATCHDOCK score as the energy function which ranks the docked models based on desolvation energy, interface area size, and geometric score.<sup>56,58</sup>

Since our peptides were designed to keep the interactions of the natural sequence of hACE2 and promote new interactions

with the RBD, for both server protocols, the following key interface amino acids were used as restraints, according to experimental data previously published:<sup>17,25,59</sup> RBD Tyr449, Tyr453, Asn487, Tyr489, Gln493, Gln498, Tyr500, Asn501 and from hACE2 Gln24, Tyr27, Lys31, His34, Glu37, Asp38, Tyr41, Gln42. Using this approach, ZDOCK and PATCHDOCK servers filter results such that only those with specified residues in the binding site are returned, focusing on the solutions that account for the known important interactions and other contacts that might arise from the modifications proposed.

#### 2.4. Docking Solutions Refinement and Validation.

Since a rigid approach was employed to generate the docking solutions and due to the fact that during protein–protein interactions, both side chains and backbone might change their conformation, we used FIBERDOCK server<sup>60</sup> for the refinement of the docking candidates. FIBERDOCK accounts for a high level of flexibility regarding protein interactions, providing a higher probability of finding a near-native conformation for the predicted solutions. The method used by FIBERDOCK models both side-chain/backbone flexibility followed by a rigid body optimization on the ligand orientation targeting the problem of flexibility and scoring of the solutions produced by ZDOCK and PATCHDOCK. This refinement algorithm mimics an induced fit process, in which the solution candidates generated previously are re-ranked according to the minimum global energy to identify suitable protein–peptide complexes.<sup>60,61</sup>

During the refinement, the following parameters were used: an antibody–antigen complex type was chosen; a restricted side-chain optimization in both receptor and ligand was performed; the Monte Carlo cycles were set to 100; an atomic radii scale of 0.95 was used. Following this first step, a second refinement was performed using the FIBERDOCK candidate with the best alignment at the interface according to the orientation of the natural hACE2 binding sequence. In this second FIBERDOCK run, we used a full side-chain optimization and the best solution from each peptide was ranked according to minimum global energy (Tables 2 and 3). The visualization of all complexes was performed using UCSF Chimera version 1.14.<sup>53</sup> The final selection of docked complexes was based on the global energy of the bound predicted complexes after the two steps of refinement and also on visual inspection to assess their spatial orientation in the interface guided by the crystal structure of the SARS-CoV-2 RBD–hACE2 complex. From that point, we selected the candidates that presented a right orientation in the interface, the lowest root-mean-square deviation (RMSD) compared to the original 22-mer peptide derived from the  $\alpha 1$  helix of hACE2, and the lowest global energy (higher stability) calculated by the scoring function of the FIBERDOCK method. The efficiency of this approach was assessed by a re-docking protocol of the original peptide sequence extracted from the crystalized hACE2 (PDB: 6M0J). Then, we analyzed the orientation in the binding site and measured the RMSD of the docked predicted 22-mer peptide derived from the  $\alpha 1$  helix of hACE2 (QAKTFLDKFNHEAEDLFYQSSL) and compared to the same structure extracted from the crystal.

**2.5. Molecular Dynamics Simulations.** MD simulations were performed to analyze the stability and dynamic properties of the RBD of the S protein bound to the most promising stapled peptides. As controls, the crystal structure of the original 22 residues from the hACE2  $\alpha 1$  helix, which lies on

**Table 2. Docking Energy Information Resulting from PATCHDOCK and Refined with FIBERDOCK<sup>a</sup>**

peptide	global energy	attractive eVdW	repulsive eVdW	ACE	HB
NYBSP-4	−54.30	−30.03	14.27	4.01	−1.94
modification 15	−51.52	−24.10	10.76	3.39	−2.40
modification 10	−49.90	−22.66	9.04	3.32	−2.35
modification 9	−49.75	−23.38	13.91	3.39	−2.06
modification 4	−49.65	−23.20	12.87	3.36	−1.60
modification 14	−49.35	−24.96	18.36	3.52	−1.83
modification 11	−49.10	−23.89	7.31	5.28	−1.06
modification 5	−48.19	−23.53	13.92	3.36	−1.66
modification 1	−46.74	−22.88	8.11	5.66	−1.52
original 3	−46.09	−23.73	12.62	6.11	−1.68
modification 6	−46.07	−23.38	9.43	5.48	−0.76
modification 2	−45.84	−22.98	10.73	5.85	−1.46
modification 3	−45.12	−24.19	9.08	6.80	−0.59
modification 13	−45.00	−25.14	9.28	6.89	−0.47
original 1	−44.65	−21.68	5.65	5.80	−1.51
original 2	−44.41	−23.27	12.57	5.97	−0.98
modification 8	−44.34	−24.48	10.67	6.90	−0.49
hACE2	−43.35	−23.34	9.09	5.63	−0.99
modification 7	−37.26	−24.58	13.72	7.67	−1.16
modification 12	−37.26	−24.58	13.72	7.67	−1.16

<sup>a</sup>Energy presented in kcal/mol; VdW: van der Waals interaction; ACE: atomic contact energy (desolvation energy); HB: hydrogen bond.

**Table 3. Docking Energy Information Resulting from ZDOCK and Refined with FIBERDOCK<sup>a</sup>**

peptide	global energy	attractive eVdW	repulsive eVdW	ACE	HB
modification 3	−53.81	−26.31	10.06	5.55	−0.20
NYBSP-4	−53.42	−25.70	12.20	2.62	−0.24
original 3	−47.75	−24.67	7.33	5.64	−0.83
modification 13	−46.60	−27.81	14.30	7.13	−2.33
hACE2	−46.49	−24.03	11.84	5.73	−1.58
modification 12	−45.84	−27.40	11.83	6.63	−0.48
modification 2	−45.20	−26.04	12.04	5.20	−0.36
modification 11	−44.65	−25.88	16.10	6.38	−0.85
modification 15	−43.90	−26.24	14.97	6.24	−0.85
modification 8	−43.15	−28.55	18.28	7.45	−0.81
modification 7	−42.91	−29.47	18.32	8.46	0.00
modification 4	−42.74	−21.60	9.25	1.99	−0.51
original 1	−42.71	−23.05	14.70	5.25	−0.97
modification 10	−41.98	−25.10	13.35	2.56	−1.60
modification 14	−41.35	−20.16	9.19	1.95	−1.00
modification 5	−39.77	−21.46	12.62	2.47	−1.30
modification 8	−39.32	−24.07	16.13	7.38	−2.22
modification 6	−38.72	−23.63	10.62	6.25	−1.00
modification 1	−38.54	−24.29	9.50	6.31	−0.95
original 2	−37.83	−20.38	5.82	5.03	−0.09
modification 9	−32.11	−19.31	7.95	1.63	−0.36

<sup>a</sup>Energy presented in kcal/mol; VdW: van der Waals interaction; ACE: atomic contact energy (desolvation energy); HB: hydrogen bond.

the interface between RBD and hACE2 (residues 24–45), and the experimentally proven antiviral NYBSP-4 double-stapled peptide were employed.

The MD simulations were conducted using Desmond version 3.0 provided with the Schrödinger package 2020–

**Table 4.** Predicted Free Energies of Binding ( $\Delta G_{\text{bind}}$ ) from the MM-GBSA Analysis and the Energy Components Used in the Calculation<sup>a</sup>

peptide	$\Delta G_{\text{bind}}$	$\Delta G_{\text{Coul}}$	$\Delta G_{\text{Cov}}$	$\Delta G_{\text{Hbond}}$	$\Delta G_{\text{Lipo}}$	$\Delta G_{\text{vdW}}$	$\Delta G_{\text{Pack}}$	$\Delta G_{\text{SolGB}}$	$\Delta G_{\text{SC}}$
Mod11	$-90.96 \pm 15.05^b$	-140.02	4.55	-6.09	-22.95	-79.72	-5.45	158.62	0.09
NYBSP-4	$-86.04 \pm 18.81^b$	-127.81	4.97	-5.72	-23.88	-78.30	-3.61	150.14	0.13
Mod15	$-81.47 \pm 9.23^b$	-82.91	5.68	-4.18	-25.95	-75.06	-5.55	106.53	-0.03
hACE2	$-75.48 \pm 10.79^b$	-123.95	0.84	-4.88	-14.90	-62.58	0.57	129.53	-0.10

<sup>a</sup>All energy terms are presented as average of all values calculated for each snapshot generated from the MD trajectory. All values are presented in kcal/mol.  $\Delta G_{\text{Coul}}$ : Coulomb energy contribution;  $\Delta G_{\text{Cov}}$ : covalent energy contribution;  $\Delta G_{\text{Hbond}}$ : hydrogen-bonding contribution;  $\Delta G_{\text{Lipo}}$ : lipophilic energy contribution;  $\Delta G_{\text{vdW}}$ : van der Waals energy contribution;  $\Delta G_{\text{Pack}}$ :  $\pi$ - $\pi$  packing energy contribution;  $\Delta G_{\text{SolGB}}$ : generalized Born electrostatic solvation energy contribution;  $\Delta G_{\text{SC}}$ : self-contact energy contribution. For more information on the energy components, see Li et al.<sup>71</sup>

<sup>b</sup>Standard deviation.

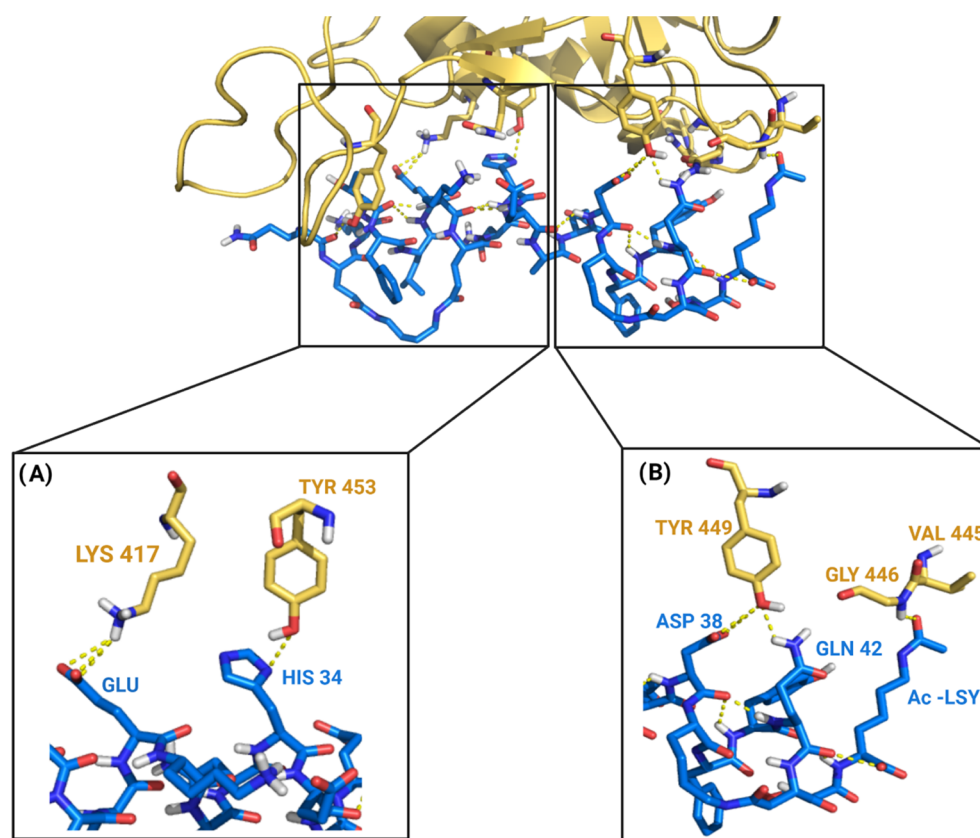


**Figure 2.** Spike protein (RBD) of SARS-CoV-2 (yellow) and modification 15 (blue) complex from PATCHDOCK prediction. (A) Detailing of the polar interactions between the substituted Glu residue and Lys417. (B) Detailing of the polar interactions determined by acetylated Lys in modification 15. The nonpolar hydrogens were hidden for visualization purpose.

4,<sup>62,63</sup> according to the following protocol: the RBD of SARS-CoV-2 bound to the designed peptide complex was placed in a cubic box with periodic boundaries and a minimum of 1 nm from any box edge to the solute. The box was filled with TIP4P water and  $\text{Na}^+$  or  $\text{Cl}^-$  ions were added, as needed by the software, to neutralize the system and to achieve a physiological concentration (150 mM). Then, the system was relaxed using the standard protocol provided in Desmond, which consists of a mixture of predefined minimizations and previous molecular dynamics executions using a constant number of particles, volume, and temperature (NVT) and a constant number of particles, pressure, and temperature (NPT) ensembles designed to slowly relax the system, while not deviating substantially from the initial protein coordinates.<sup>63</sup> After, the simulations for all systems were performed under NPT ensemble with the temperature set to 300 K and

the pressure set to 1.013 bar using the Nosé–Hoover<sup>64</sup> and the Martyna–Tobias–Klein<sup>65</sup> algorithms. Production of MD simulations was set to 500 ns, and they were performed using Desmond GPU with the OPLS3e force field<sup>66</sup> through the Holland Computing Center.<sup>67</sup> The OPLS3e force field<sup>66</sup> is based on the optimized potentials for liquid simulations (OPLS) first developed by Jorgensen and co-workers.<sup>68</sup> OPLS3e displays significant improvements in the representation of secondary structure elements in simulated peptides and native structure stability over a number of proteins.<sup>66</sup>

Finally, the root-mean-square deviation (RMSD) for both protein and peptide ligands, after MD simulations, were evaluated to understand the relative stabilities of the complexes. In addition, the trajectories of the most promising complexes were analyzed and recorded in video format using the Maestro interface from the Schrödinger package 2020–



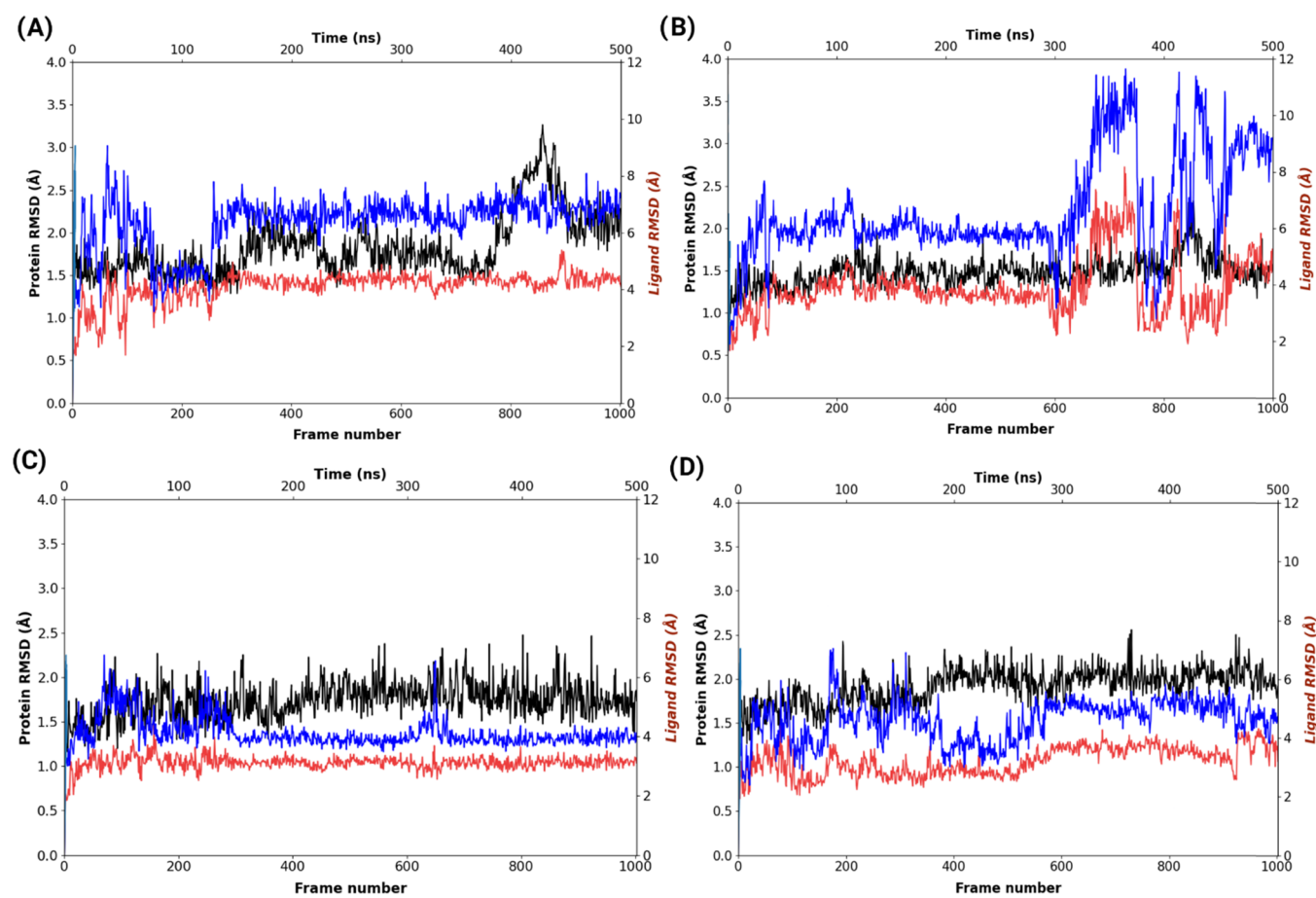


**Figure 3.** RMSD fluctuations of the original 22-mer hACE2  $\alpha$ 1 helix (A), NYBSP-4 stapled control (B), modification 15 (C), and modification 11 (D) spike protein of SARS-CoV-2 complexes. The 500 ns MD simulations were monitored with the first frame as a reference. RMSD based on carbon  $\alpha$  of the protein (black) (left Y-axis) and ligand RMSD (right Y-axis). Lig fit Prot in blue, and Lig fit Lig in red.

4.<sup>62,63</sup> The protein–stapled peptide interactions were monitored as well during the entire period of the simulation. Then, the interactions between the RBD of SARS-CoV-2 and the stapled peptides were analyzed using the analyze trajectory script<sup>69</sup> provided by Schrödinger, which reads a trajectory file and identifies interactions occurring between the defined sets.

**2.6. Binding Free Energy Analysis.** The estimation of the free energies for the binding between the RBD of SARS-CoV-2 and the most promising stapled peptide complexes ( $\Delta G_{\text{bind}}$  in kcal/mol), according to the analysis of the MD results, were computed using the molecular mechanics with generalized Born and surface area (MM/GBSA)<sup>70</sup> continuum solvation method<sup>71</sup> implemented in the Schrödinger package. The MM-GBSA binding free energy was estimated as follows:  $\Delta G_{\text{bind}} = G_{\text{complex}} - G_{\text{receptor}} - G_{\text{ligand}}$ , where  $\Delta G_{\text{bind}}$  is the binding free energy and  $G_{\text{complex}}$ ,  $G_{\text{receptor}}$ , and  $G_{\text{ligand}}$  are the free energies of complex, receptor, and ligand, respectively. The thermal MM-GBSA script provided by Schrödinger<sup>69,71</sup> was used to calculate the  $\Delta G_{\text{bind}}$  for the studied complexes. This script takes in a Desmond MD trajectory, splits it into individual frame snapshots, and runs each one through MM-GBSA analysis. During the MM-GBSA calculation, 702 snapshots from the 500 ns MD simulation were used as input to compute the average binding free energy. The predicted free energies of binding are presented as average values ( $\Delta G_{\text{bind}}$ , Table 4) along with the energy components used in the calculation.

### 3. RESULTS AND DISCUSSION

**3.1. Docking Results.** The results for the PATCHDOCK/FIBERDOCK and ZDOCK/FIBERDOCK studies are presented in Tables 2 and 3, respectively. As it can be seen, for the first approach several proposed modifications presented a lower global energy (higher stability) compared to the sequence derived from the  $\alpha$ 1 helix of hACE2 (QAKTFLDKFNHEAEDLFYQSSL). Only two proposed modifications showed higher energies than the original sequence (modification 7 and 12). Regarding the second approach, only three proposed stapled peptides showed better energy results compared to the hACE2 original sequence. Additionally, for both docking servers, our best ranked stapled peptides present docking scores similar to the scores of the control NYBSP-4 (experimentally proven SARS-CoV-2-RBD peptide binder<sup>40</sup>). For the PATCHDOCK study, the best proposed peptide (modification 15) shows a docking score of  $-51.52$  kcal/mol, while NYBSP-4 presents  $-54.30$  kcal/mol. For the ZDOCK approach, the best docking solution (modification 3) presents a docking score slightly better ( $-53.81$  kcal/mol) than the NYBSP-4 peptide ( $-53.42$  kcal/mol). These findings suggest that the highest-ranked docking solutions from our study are comparable to the control in affinity toward the RBD of SARS-CoV-2.

Comparing the results of the two docking approaches indicates that even though the overall energies are similar ( $-51.52$  kcal/mol for the best solution using the PATCH-

DOCK protocol and  $-53.81$  kcal/mol for ZDOCK best's solution), the top-ranked candidates are distinct for each method. This divergence reflects the distinct methods employed to generate the docking poses in each server.

Regarding the top predicted candidates from the PATCHDOCK protocol, the replacement of Leu45 by K(Ac) may increase the affinity for the SARS-CoV-2 RBD since all top 3 ranked predictions (modifications 15, 10, and 9) present this modification (Figures S1 and 2B). This change allows an additional hydrogen bond with Gly446 in the RBD increasing the affinity to the S protein. Additionally, the substitution of Asp30 by a Glu seems to favor the affinity between the systems since the top 2 ranked solutions present this designed replacement (Figure 2A). These observations help to explain the superior hydrogen-bond energy contribution of these structures compared to the hACE2 peptide ( $-2.40$ ,  $-2.35$ , and  $-2.06$  kcal/mol of the top 3 predictions vs  $-0.99$  kcal/mol in hACE2).

As for the ZDOCK top predictions, the Asp30 substitution by Glu also seems to play an important role in the predicted binding affinity since modifications 3 and 13 show this feature (Figure S1, SI). Another interesting point from the ZDOCK solutions is the fact that two out of the three top-ranked stapled peptides present a double-lactam bridge between Ala25 and Phe32 (modification 13 and original 3, Figures 1 and S1). The same type of staple is also present in the top candidate from PATCHDOCK protocol (modification 15), which indicates the positive effect of this modification in the top predictions.

**3.2. Re-docking Evaluation.** Regarding the re-docking protocol employing the original 22 amino acids from hACE2, the overall procedure was considered satisfactory after the RMSD analysis. According to the Critical Assessment of PRediction of Interactions (CAPRI)-inspired threshold for success,<sup>72</sup> a docking protocol finds a near-native conformation if the peptide lies within  $4.0$  Å backbone RMSD of the native peptide bound to the receptor (*i.e.*, the CAPRI criterion for an acceptable peptide–protein docking prediction). The prediction made by ZDOCK server produced a docking solution for the original structure with an RMSD calculated of  $2.782$  Å, compared to the crystal structure. After the two refinement steps using FIBERDOCK, the best obtained prediction presented an RMSD of  $0.556$  Å (Figure S3, SI). For the PATCHDOCK server, the best predicted solution presented an RMSD of  $3.144$  Å, and after the use of FIBERDOCK, the difference was  $0.373$  Å (Figure S3, SI). Therefore, we concluded the docking protocol is suitable for producing acceptable peptide–protein docking predictions regarding this specific complex, and the refinement process can improve the quality of the prediction. The low RMSD obtained with both methods reinforce the likelihood of the approach in producing predictions close to a native conformation.<sup>58</sup>

**3.3. Molecular Dynamics Simulation Analysis.** MD determines, *in silico*, how motion can affect protein–peptide interactions, the stability of those complexes, and their conformation variations due to binding.<sup>73,74</sup> The first parameter analyzed from the MD trajectories was the RMSD, which measures the average distance between a group of atoms.<sup>75</sup> Analysis of this parameter during the simulation time allows us to determine the level of protein or peptide conformational changes. Monitoring the RMSD of the protein (left Y-axis in Figure 3, black lines) can provide an understanding of the structural conformation of the studied

protein, giving insights into the stability. Ligand RMSD (right Y-axis in Figure 3, blue and red lines) is an indication of ligand stability with respect to the protein, as well as the evolution of its internal conformation. Promising inhibitors should have low RMSDs during the simulation.<sup>76</sup>

Based on the RMSDs values and RMSD standard deviation for the complexes composed of the spike protein and top-ranked docking candidates (Table S1, SI), the complex S protein–modification 15 (best docking prediction from PATCHDOCK web server) showed the best results (Figure 3). As it can be seen in Figure 3 and Table S1 (SI), when analyzed together, the ligand RMSD (“Lig fit Prot” and “Lig fit Lig”) and the standard deviation values for modification 15 complex presented the lowest values. As presented in the plots in Figure 3, this complex displays a very stable profile along the 500 ns trajectory. Modification 11 also displays a stable profile with low values for ligand RMSD and ligand RMSD standard deviation. The protein RMSD (Table S1 and Figure 3) for these complexes reveals a stable profile, even though considering the average value for this parameter, the complexes with modification 15 and modification 11 do not present the lowest values (see Table S1 (SI), Prot CA column). Furthermore, these cited complexes perform better in the RMSD overall analysis than the original 22 residues from the hACE2  $\alpha 1$  helix, NYBSP-4, and the modification 3 complex (best docking prediction from ZDOCK web server, Figure S4, SI).

The Lig fit Prot (blue lines in Figure 3) represents the RMSD of a ligand when the protein–ligand complex is first aligned on the protein backbone and then the RMSD of the ligand heavy atoms is measured. If the values observed are significantly larger than the RMSD of the protein, then it is likely that the ligand has diffused away from its initial binding,<sup>76</sup> which can be observed for modification 14, original 3, and modification 9 (Figure S4, SI). In the case of modification 15, this parameter suffers fluctuations during the simulation, especially at the beginning of the trajectory until the equilibration of the system; then, it maintains stability throughout the end of the simulation.

Furthermore, the Lig fit Lig (red lines in Figure 3) shows the RMSD of a ligand that is aligned and measured just on its reference conformation (frame 1 in this case). Regarding this parameter, considering both the average Lig fit Lig RMSD value and the standard deviation, modification 15 and modification 11 complexes showed the best results of all studied complexes. Notably, for these cited complexes, the Lig fit Lig RMSD reveals a stable profile of its ligand atoms internal fluctuations ( $3.11 \pm 0.23$  Å for modification 15 and  $3.20 \pm 0.48$  Å for modification 11 against  $4.10 \pm 0.51$ ,  $3.87 \pm 1.00$ , and  $3.76 \pm 0.42$  Å for hACE2 control, NYBSP-4, and modification 3, respectively). The RMSD and standard deviation values for the others studied peptides are presented in the SI (Table S1 and Figure S4).

The superior stability, based on ligand RMSDs values, especially for modification 15 but also observed for the other stapled peptides tested (Table S1, SI), compared to the hACE2 control, can be attributed to the staples present in these structures. The presence of the two staples resulted in the maintenance of the  $\alpha$ -helical character (key for the interaction of hACE2 with the RBD<sup>7</sup>) along the trajectory. The ability to maintain the secondary structure during most of the simulation time, despite some occasional fluctuations, can be observed in the movie generated from the MD simulation



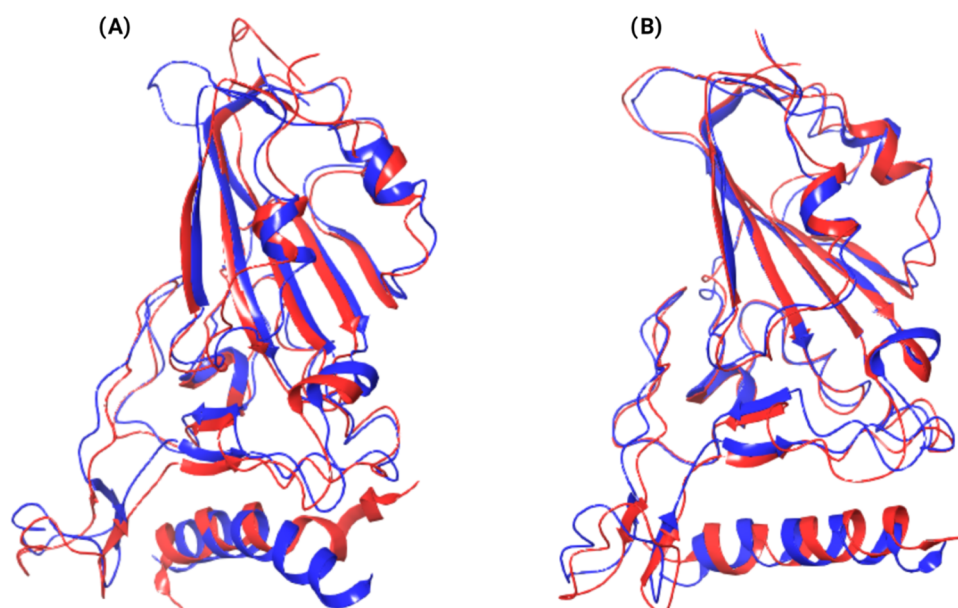


**Figure 4.** Superimposition of the initial structure (red) and final structure (blue) after 500 ns of simulation of the SARS-CoV-2 spike protein bound to (A) control  $\alpha$ 1 helix and (B) designed peptide modification 15.

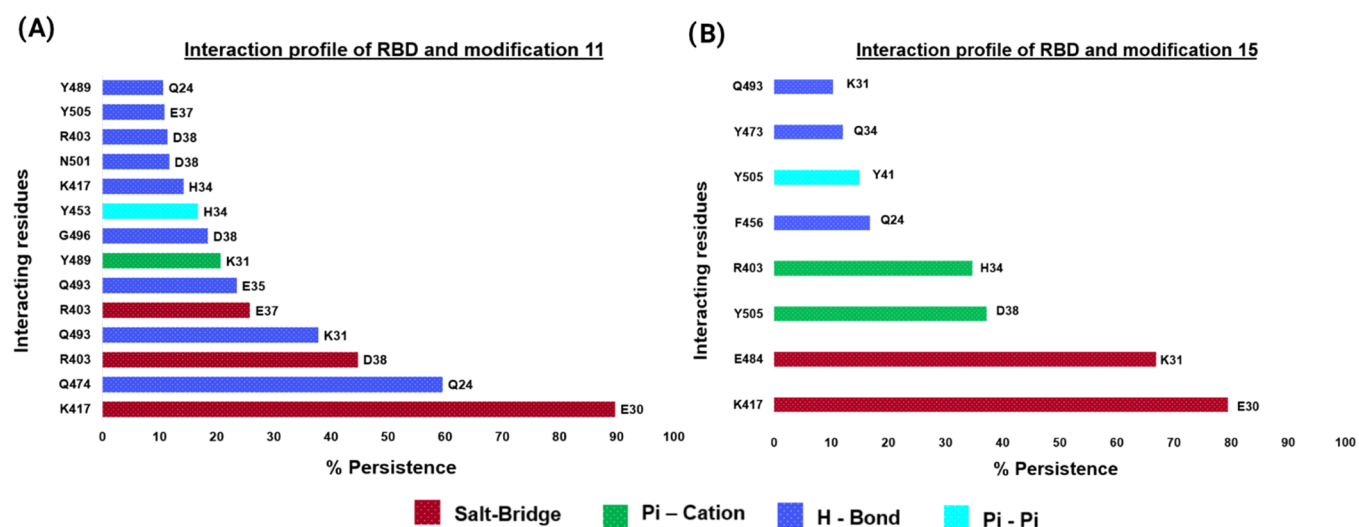


**Figure 5.** Most persistent interactions (>10% of simulation time) from modification 11 (A) and modification 15 (B) with SARS-CoV-2 RBD. Interacting residues from RBD of SARS-CoV-2 (left Y-axis) and from the studied stapled peptides (right Y-axis).

trajectory of modification 15 (Movie S1, SI). The same feature is not present in the control hACE2 (Movie S2, SI) or even in modification 3 (Movie S3, SI). Additionally, modification 15 also performs better in the RMSD stability analysis compared to modification 10 and original 3 (second best docking candidates from PATCHDOCK and ZDCOK server, respectively, Figure S4 and Table S1, SI). In summary, the RBD-modification 15 complex was the best solution, showing a stable RMSD profile for both protein and ligand evaluations, and reaching the equilibrium state at the end of the MD simulation despite some occasional oscillations along the process. Modification 11 also performed well in the stability analysis, which supports both structures as potential RBD inhibitors.

At the time of this study and to the best of our knowledge, three reports by Curreli et al.,<sup>40</sup> Maas et al.,<sup>41</sup> and Morgan et al.<sup>42</sup> described the design and synthesis of stapled peptides also

based on the native hACE2  $\alpha$ 1 helix. In the first report, a pseudoviral assay showed that a 30-mer double-hydrocarbon-stapled peptide effectively inhibited viral entry. Maas et al.<sup>41</sup> predicted that 35-mer lactam-stapled peptides can inhibit the S protein RBD–hACE2 complex formation. However, the last study pointed out that mono-stapled peptides can successfully constrained  $\alpha$ -helical structure in solution but do not prevent virus internalization. Thus, according to the suggestion by Morgan et al.,<sup>42</sup> the double stapling is a viable approach for inducing  $\alpha$ 1-helicity, which may prevent virus internalization as described by Curreli et al.<sup>40</sup> when smaller peptides ( $\sim$ 30 mer) are evaluated. Therefore, it is possible to assume that a double-stapled approach, as the one we describe here, compass a superior strategy to develop shorter stapled peptides based on the hACE2 as a new therapeutic to prevent viral infection.

The antiviral activity and superior  $\alpha$ -helicity observed in the experimental study of Curreli et al.<sup>40</sup> (which possess a double-

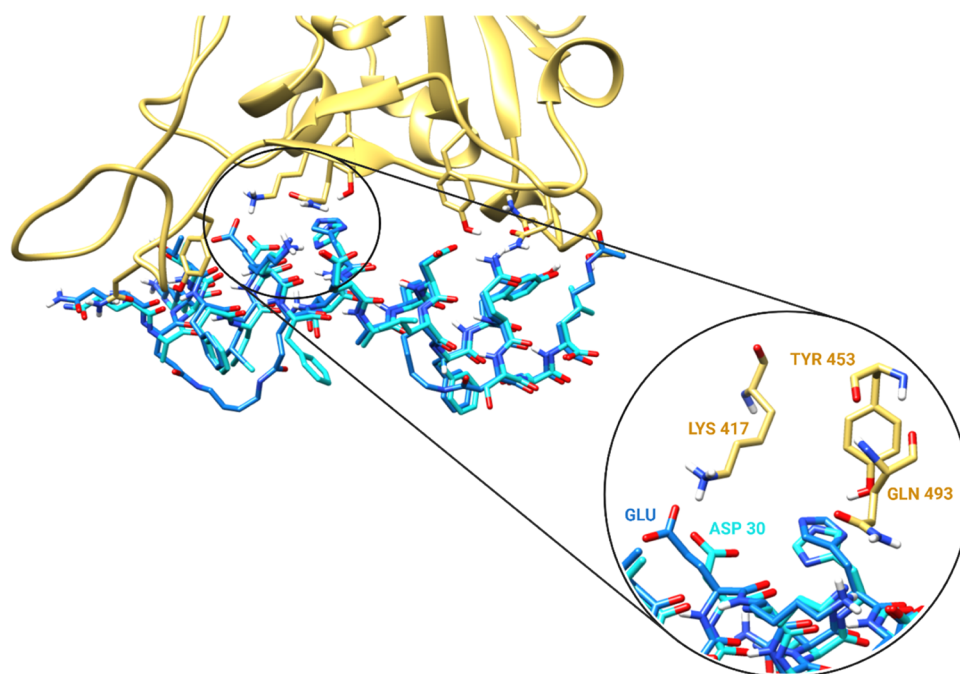


**Figure 6.** Detailing of the aspartic acid 30 substitution by glutamic acid in modification 15. Spike protein (RBD) of SARS-CoV-2 (yellow). Modification 15 (blue) and hACE2 control (cyan) overlaid. The nonpolar hydrogens were hidden for visualization purpose.

stapled) might be partly understood by the results of our MD simulation study. According to Figure 4, in which the initial and final structures from the MD studies of the control peptide and modification 15 are superimposed, the second stapled at the right side of the designed peptide helps to sustain this part of the structure in place in the complex with the S protein. This prevents the designed peptide from moving around and also to maintain the  $\alpha$ -helicity of this side of the structure in place during the simulation. Thus, it can be theorized that the second staple prevents slight rotations of the  $\alpha$  helix segments, which can lower affinity. These observations can also be seen in Movies S1, S4, and S5, SI. It is noteworthy to mention that most of our proposed modifications contain lactam bridges, which should be less lipophilic than a staple peptide containing an alkene group.

**3.4. Protein–Stapled Peptide Interactions Obtained from MD Simulation.** The important interactions (more than 10% persistence) between the RBD of SARS-CoV-2 and modification 15 or 11 from the MD trajectory are shown in Figure 5. For modification 15/RBD complex, the amino acids Lys417, Glu484, and Tyr505 (RBD) and Glu30, Lys31, and Asp38 (peptide) exhibited the most remarkable interactions over the 500 ns simulation period. For modification 11/RBD complex, the residues Lys417, Gln474, Arg403, Gln493, and Tyr489 (RBD) and Glu30, Gln24, Asp38, and Lys31 (peptide) are particularly important for the interaction between the S protein and this stapled peptide.

One interesting feature of modification 15 and modification 11 interaction profiles is the persistence of the most important interaction during the simulation time (Figure 5). This interaction is represented by a salt–bridge between Lys417 in the RBD and the substituted Glu residue from our stapled peptides (89.72 and 79.40% of persistence in the simulation time for modifications 11 and 15, respectively). This fact is particularly relevant when analyzed according to the report of Ghorbani et al.<sup>77</sup> In such a study, the binding free energy for

the SARS-CoV-2 and RBD interaction were decomposed into a per-residue-based binding energy to find the residues that contribute strongly to the binding and are responsible for the higher binding affinity of SARS-CoV-2 for the hACE2 compared to SARS-CoV. Among their findings, the authors point out that from all of the interface residues, Lys417 had the highest contribution to the total binding energy ( $-12.34 \pm 0.23$  kcal/mol) by interacting with Asp30 from hACE2 (also *via* a salt–bridge). The same salt–bridge interaction between Lys417 and Asp30 from our control hACE2 shows less than half of the persistence value (35.22%) of our studied stapled peptides. Regarding the control NYBSP-4, the persistence for the interaction Lys417 and Asp30 is 74.75%. This observation directed us to conclude that: (i) the presence of two staples in modification 15, modification 11, and the control NYBSP-4 helps to maintain the bioactive conformation allowing the interacting residues to stay in the right position to determine interactions with their partner residues in the viral RBD. This ability is lost in the nonstapled control hACE2 used here; (ii) substitution of Asp30 in modifications 15 and 11 by a Glu30 is effective in placing this residue closer to its partner interacting residue (Lys417). This substitution leads to an increased interaction persistence along the simulation compared to the controls, which possess an Asp30 in the same position (Figure 6). The interaction profile of the controls is available in Table S2, SI.

**3.5. Stability and Profile Interaction in the Presence of E484K RBD Mutation.** The second most important interaction of modification 15 is a salt–bridge between Glu484 (RBD) and Lys31. According to the CDC, laboratory studies suggest that specific monoclonal antibody treatments may be less effective for treating cases of COVID-19 caused by variants with the E484K substitution in the spike protein.<sup>51,78–80</sup> Additionally, there are three circulating variants of concern, which present such mutation: B.1.351 lineage (also known as (a.k.a.) 20H/501Y.V2) first described in South Africa;<sup>81</sup> P.1

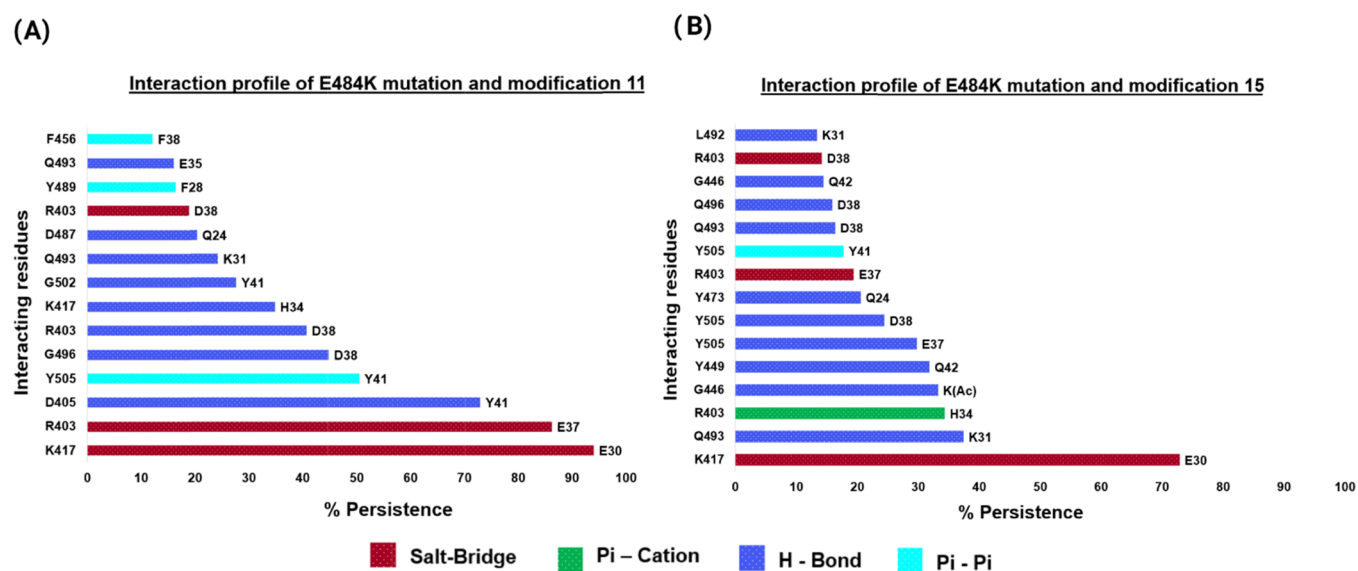


**Figure 7.** Most persistent interactions (>10% of simulation time) from modification 11 (A) and modification 15 (B) with viral RBD containing the mutation E484K. Interacting residues from RBD of SARS-CoV-2 (left Y-axis) and from modification 15 (right Y-axis).

lineage (a.k.a. 20J/501Y.V3) first reported in Japan in four travelers from Brazil,<sup>82,83</sup> and finally, the B.1.1.7 lineage (a.k.a. 20I/501Y.V1) first detected in the United Kingdom<sup>84</sup> (this mutation is found in some but not all sequences<sup>51</sup>). Therefore, we decided to analyze the interaction profile and stability of modification 15 in the presence of the spike protein RBD presenting the E484K mutation. Even though this specific interaction does not show a relevant persistence (>10%) in the interaction profile of modification 11 and the viral RBD, we decided to analyze the behavior of this peptide in the presence of the cited mutation. This was done with the purpose to assess if the stable profile demonstrated by this stapled peptide in the simulation would be somehow affected by the presence of SARS-CoV-2 variants presenting this mutation.

The ligand RMSD values calculated from the MD trajectory of E484K-mutated RBD/modification 15 and 11 reveal stable profiles of the peptides with respect to the protein and to their internal fluctuations (Figure S5). Specifically, modification 15 presented the following values for the Lig fit Prot and Lig fit Lig RMSD:  $4.26 \pm 0.43$  and  $3.46 \pm 0.25$  Å. For modification 11, the values for the same parameters are:  $4.76 \pm 0.59$  and  $3.19 \pm 0.51$  Å. These ligand RMSD and standard deviation values for the mutated complexes are comparable to the values seen in the original RBD and the same stapled peptides. As presented in Table S1 (SI), the original RBD/modification 15 shows  $4.12 \pm 0.49$  and  $3.11 \pm 0.23$  Å and RBD/modification 11 shows  $4.57 \pm 0.72$  and  $3.20 \pm 0.48$  Å for the same parameters. Overall, both mutated RBD and stapled peptide complexes present better stability profiles than the hACE2  $\alpha 1$  helix control and the stapled NYBSP-4 control (RMSD plot for the tested stapled peptides and mutated RBD trajectories are presented in Figure S5, and RMSD for the controls is shown in Figure 3 and Table S1).

Important interactions between the mutated RBD of SARS-CoV-2 and the tested peptides are shown in Figure 7. The interaction profile of modification 15 and mutated RBD shows a shift in the character of the major interaction types compared to the trajectory of the natural RBD/modification 15 complex (see Figures 5B and 7B). In the trajectory resulting from the MD simulation of modification 15 and the natural RBD, the

most important interaction type is represented by salt-bridge interactions with high persistence (Lys417/substituted Glu: 79.40%; Glu484/Lys31: 66.80%). However, in the E484K-mutated RBD and modification 15 complex, the interactions of this specific type have reduced persistence (Figure 7B). To compensate this reduction, increased number of hydrogen-bond (H-bond) interactions are displayed presenting lower persistence. This increase in the H-bond interactions must contribute to the good stability of modification 15/E484K-mutated RBD complex, as demonstrated by the stable profile seen in the RMSD parameters. Note that even though the salt-bridge interactions have a lower influence in the interaction profile of modification 15 and mutated RBD, the interaction between Lys417 and substituted Glu30 suffers a low reduction in the persistence displaying a value of 72.85%.

Furthermore, for modification 11-mutated RBD complex, some interactions were lost, and some were created (see Figures 5A and 7A), leading to an interaction profile with the same number of contacts presented by the natural complex. The most remarkable difference is the appearance of a new salt-bridge between Arg403 and Glu37 in the mutated complex with a persistence of 86.20% (Figure 7A). Similarly to modification 15, the analysis of persistence for the salt-bridge interaction between Lys417 and substituted Glu in modification 11 shows a maintenance of this important interaction. Interestingly, the mutated complex shows a slightly increasing in persistence going from 89.72% in the original RBD/peptide interaction to 94.01% in the mutated complex. Together these results lead us to hypothesize that the E484K mutation present in different SARS-CoV-2 lineages will not hamper the ability of modification 15 or modification 11 to bind the viral RBD.

**3.6. Binding Free Energy Analysis.** Molecular docking provides a fast/efficient way to predict protein-protein interactions (PPIs) and to rank them accordingly to the docking score.<sup>85</sup> However, most scoring functions used by docking programs are developed to enhance computational efficiency and, consequently, present a reduced accuracy of prediction.<sup>86</sup> Methods that combine molecular mechanics energy and implicit solvent models such as MM/GBSA are



theoretically more rigorous than docking scoring functions and are powerful tools to predict the binding affinities for protein–peptide systems.<sup>86,87</sup> To predict the binding affinity of our proposed peptides to the RBD of SARS-CoV-2 and to compare this predicted binding affinity with the experimentally validated NYBSP-4, the MM/GBSA calculation was employed. The results of such analysis are presented in Table 4 for the controls, modification 15, and modification 11, and in Table S3 (SI) for the other best docking ranked stapled peptides.

According to the results presented in Table 4, modification 11 is predicted to have better binding affinity to the viral RBD. Interestingly, this modification exhibits superior predicted affinity compared to the experimentally validated NYBSP-4. In addition, NYBSP-4 has a slightly better binding affinity compared to modification 15. However, NYBSP-4 is a longer peptide (30-mer stapled peptide) than both modification 15 and modification 11 (22-mer stapled peptides). Moreover, modifications 15 and 11 being smaller structures can be easier and cheaper to prepare. Further, both of our proposed stapled peptides should provide a better water solubility profile.

Overall, modification 15 and modification 11 showed good stability results for the parameters analyzed in this study. Modification 11 showed better results in the binding free energy prediction calculated using the MM-GBSA method. Furthermore, modification 15 displays a predicted binding affinity comparable to the control NYBSP-4 when analyzed accordingly to their size. Additional experimental studies are required to determine the activity of these peptides against SARS-CoV-2. Nevertheless, our *in silico* study provide initial evidence to confirm that double-stapled peptides derived from the hACE2  $\alpha$ 1 helix present a therapeutic strategy worthy of further investigation.

#### 4. CONCLUSIONS

Through the use of structure-based design, it was possible to propose 18 (22-mer) stapled peptides derived from the hACE2  $\alpha$ 1 helix. These peptides were designed to retain the  $\alpha$ -helical character of the natural structure, to have enhanced binding affinity between the peptides and SARS-CoV-2-RBD, to avoid disrupting existing favorable interactions, and to display a better solubility profile compared to bigger stapled peptides available in the literature. Furthermore, using docking techniques and a refinement protocol, we selected the most promising binders to perform further analysis using MD simulation and MM-GBSA free energy of binding prediction. According to our study, we identified modifications 11 and 15 as our best candidates. We predict that these peptides can bind to SARS-CoV-2-RBD with potency higher than or similar to the control NYBSP-4 (experimentally proven SARS-CoV-2-RBD 35-mer peptide binder) showing the advantages of being smaller peptides. Our most promising stapled peptides showed stable profiles in the MD simulation and could retain important interactions with the RBD even in the presence of the E484K RBD mutation. Moreover, our study provides valuable information for the rational design and development of stapled peptide inhibitors against SARS-CoV-2 infection.

#### ■ ASSOCIATED CONTENT

##### SI Supporting Information

The Supporting Information is available free of charge at <https://pubs.acs.org/doi/10.1021/acs.jpcb.1c02398>.

Two-dimensional structures of the designed stapled peptides; schematic representation of SARS-CoV-2 RBD from the spike protein and hACE2 receptor; 22-mer hACE2 from  $\alpha$ 1 helix crystallized structure overlaid with the docking prediction of the same structure for PATCHDOCK and ZDOCK servers; RMSD fluctuations of the spike protein and modification 4, modification 14, modification 13, original 3, modification 10, modification 9, and modification 3; RMSD fluctuations of the E484K-mutated spike protein and modification 11 and modification 15; RMSD values (Å) for the studied complexes; main interactions (>10% of persistence) between SARS-CoV-2 and the controls; and predicted free energies of binding ( $\Delta G_{\text{bind}}$ ) from the MM-GBSA analysis (PDF)

MD simulation trajectory of modification 15 (Movie S1) (MP4)

MD simulation trajectory of modification hACE2 (Movie S2) (MP4)

MD simulation trajectory of modification 3 (Movie S3) (MP4)

MD simulation trajectory of modification NYBSP-4 (Movie S4) (MP4)

MD simulation trajectory of modification 11 (Movie S5) (MP4)

#### ■ AUTHOR INFORMATION

##### Corresponding Author

**Martin Conda-Sheridan** – Department of Pharmaceutical Sciences, College of Pharmacy, University of Nebraska Medical Center, Omaha, Nebraska 68198, United States; [orcid.org/0000-0002-3568-2545](https://orcid.org/0000-0002-3568-2545); Phone: +1-402-559-9361; Email: [martin.condasheridan@unmc.edu](mailto:martin.condasheridan@unmc.edu)

##### Authors

**Luana Janaína de Campos** – Department of Pharmaceutical Sciences, College of Pharmacy, University of Nebraska Medical Center, Omaha, Nebraska 68198, United States  
**Nicholas Y. Palermo** – Computational Chemistry Core Facility, Vice Chancellor for Research Cores, University of Nebraska Medical Center, Omaha, Nebraska 68198, United States

Complete contact information is available at: <https://pubs.acs.org/10.1021/acs.jpcb.1c02398>

##### Author Contributions

M.C.-S. conceived the idea and designed the peptides. L.J.d.C. also designed peptides and run the docking and MD studies. N.Y.P. performed initial MD simulations. All authors wrote and reviewed the manuscript.

##### Notes

The authors declare no competing financial interest.

#### ■ ACKNOWLEDGMENTS

The authors gratefully acknowledge the computing resources provided by the University of Nebraska Lincoln's Holland Computing Center. This research was supported by startup funds from UNMC (M.C.-S.). In addition, the final assembly of the figures displayed in this paper was created with the BioRender.com website.

## REFERENCES

- (1) Wang, C.; Horby, P. W.; Hayden, F. G.; Gao, G. F. A Novel Coronavirus Outbreak of Global Health Concern. *Lancet* **2020**, *395*, 470–473.
- (2) Kalathiya, U.; Padariya, M.; Mayordomo, M.; Lisowska, M.; Nicholson, J.; Singh, A.; Baginski, M.; Fahraeus, R.; Carragher, N.; Ball, K.; et al. Highly Conserved Homotrimer Cavity Formed by the Sars-Cov-2 Spike Glycoprotein: A Novel Binding Site. *J. Clin. Med.* **2020**, *9*, 1473–1491.
- (3) World Health Organization. Weekly Operational Update on Covid-19—17 May 2021. <https://www.who.int/publications/m/item/weekly-operational-update-covid-19--17-may-2021> (accessed May 18, 2021).
- (4) Hartley, D. M.; Perencevich, E. N. Public Health Interventions for Covid-19: Emerging Evidence and Implications for an Evolving Public Health Crisis. *JAMA* **2020**, *323*, 1908–1909.
- (5) Nicola, M.; Alsaifi, Z.; Sohrabi, C.; Kerwan, A.; Al-Jabir, A.; Iosifidis, C.; Agha, M.; Agha, R. The Socio-Economic Implications of the Coronavirus Pandemic (Covid-19): A Review. *Int. J. Surg.* **2020**, *78*, 185–193.
- (6) Ioannides, D.; Gyimóthy, S. The Covid-19 Crisis as an Opportunity for Escaping the Unsustainable Global Tourism Path. *Tourism Geogr.* **2020**, *22*, 624–632.
- (7) Han, Y.; Král, P. Computational Design of Ace2-Based Peptide Inhibitors of Sars-Cov-2. *ACS Nano* **2020**, *14*, 5143–5147.
- (8) Astuti, I. Ysrafil Severe Acute Respiratory Syndrome Coronavirus 2 (Sars-Cov-2): An Overview of Viral Structure and Host Response. *Diabetes Metab. Syndr.: Clin. Res. Rev.* **2020**, *14*, 407–412.
- (9) Liu, C.; Yang, Y.; Gao, Y.; Shen, C.; Ju, B.; Liu, C.; Tang, X.; Wei, J.; Ma, X.; Liu, W.; et al. Viral Architecture of Sars-Cov-2 with Post-Fusion Spike Revealed by Cryo-EM. *bioRxiv* **2020**, No. 2020.03.02.972927.
- (10) Walls, A. C.; Xiong, X.; Park, Y. J.; Tortorici, M. A.; Snijder, J.; Quispe, J.; Cameroni, E.; Gopal, R.; Dai, M.; Lanzavecchia, A.; et al. Unexpected Receptor Functional Mimicry Elucidates Activation of Coronavirus Fusion. *Cell* **2019**, *176*, 1026–1039.
- (11) Yuan, M.; Wu, N. C.; Zhu, X.; Lee, C.-C. D.; So, R. T. Y.; Lv, H.; Mok, C. K. P.; Wilson, I. A. A Highly Conserved Cryptic Epitope in the Receptor Binding Domains of Sars-Cov-2 and Sars-Cov. *Science* **2020**, *368*, 630–633.
- (12) Li, H.; Liu, S. M.; Yu, X. H.; Tang, S. L.; Tang, C. K. Coronavirus Disease 2019 (Covid-19): Current Status and Future Perspectives. *Int. J. Antimicrob. Agents* **2020**, *55*, No. 105951.
- (13) Wrapp, D.; Wang, N.; Corbett, K. S.; Goldsmith, J. A.; Hsieh, C. L.; Abiona, O.; Graham, B. S.; McLellan, J. S. Cryo-Em Structure of the 2019-Ncov Spike in the Prefusion Conformation. *Science* **2020**, *367*, 1260–1263.
- (14) Zhou, P.; Yang, X. L.; Wang, X. G.; Hu, B.; Zhang, L.; Zhang, W.; Si, H. R.; Zhu, Y.; Li, B.; Huang, C. L.; et al. A Pneumonia Outbreak Associated with a New Coronavirus of Probable Bat Origin. *Nature* **2020**, *579*, 270–273.
- (15) Hoffmann, M.; Kleine-Weber, H.; Schroeder, S.; Krüger, N.; Herrler, T.; Erichsen, S.; Schiergens, T. S.; Herrler, G.; Wu, N. H.; Nitsche, A.; et al. Sars-Cov-2 Cell Entry Depends on Ace2 and Tmprss2 and Is Blocked by a Clinically Proven Protease Inhibitor. *Cell* **2020**, *181*, 271–280.
- (16) Ortega, J. T.; Serrano, M. L.; Pujol, F. H.; Rangel, H. R. Role of Changes in Sars-Cov-2 Spike Protein in the Interaction with the Human Ace2 Receptor: An in Silico Analysis. *Excli J.* **2020**, *19*, 410–417.
- (17) Yan, R.; Zhang, Y.; Li, Y.; Xia, L.; Guo, Y.; Zhou, Q. Structural Basis for the Recognition of Sars-Cov-2 by Full-Length Human Ace2. *Science* **2020**, *367*, 1444–1448.
- (18) Ponga, M. Quantifying the Adhesive Strength between the Sars-Cov-2 S-Proteins and Human Receptor and Its Effect in Therapeutics. *Sci. Rep.* **2020**, *10*, No. 17538.
- (19) Prajapat, M.; Sarma, P.; Shekhar, N.; Avti, P.; Sinha, S.; Kaur, H.; Kumar, S.; Bhattacharyya, A.; Kumar, H.; Bansal, S.; et al. Drug Targets for Corona Virus: A Systematic Review. *Indian J. Pharmacol.* **2020**, *52*, 56–65.
- (20) Du, L.; He, Y.; Zhou, Y.; Liu, S.; Zheng, B. J.; Jiang, S. The Spike Protein of Sars-Cov-a Target for Vaccine and Therapeutic Development. *Nat. Rev. Microbiol.* **2009**, *7*, 226–236.
- (21) Xia, S.; Liu, M.; Wang, C.; Xu, W.; Lan, Q.; Feng, S.; Qi, F.; Bao, L.; Du, L.; Liu, S.; et al. Inhibition of Sars-Cov-2 (Previously 2019-Ncov) Infection by a Highly Potent Pan-Coronavirus Fusion Inhibitor Targeting Its Spike Protein That Harbors a High Capacity to Mediate Membrane Fusion. *Cell Res.* **2020**, *30*, 343–355.
- (22) Pandey, P.; Rane, J. S.; Chatterjee, A.; Kumar, A.; Khan, R.; Prakash, A.; Ray, S. Targeting Sars-Cov-2 Spike Protein of Covid-19 with Naturally Occurring Phytochemicals: An in Silico Study for Drug Development. *J. Biomol. Struct. Dyn.* **2020**, 1–11.
- (23) Zhang, G.; Pomplun, S.; Loftis, A. R.; Loas, A.; Pentelute, B. L. The First-in-Class Peptide Binder to the Sars-Cov-2 Spike Protein. *bioRxiv* **2020**, No. 2020.03.19.999318.
- (24) Ho, T. Y.; Wu, S. L.; Chen, J. C.; Wei, Y. C.; Cheng, S. E.; Chang, Y. H.; Liu, H. J.; Hsiang, C. Y. Design and Biological Activities of Novel Inhibitory Peptides for Sars-Cov Spike Protein and Angiotensin-Converting Enzyme 2 Interaction. *Antiviral Res.* **2006**, *69*, 70–76.
- (25) Lan, J.; Ge, J.; Yu, J.; Shan, S.; Zhou, H.; Fan, S.; Zhang, Q.; Shi, X.; Wang, Q.; Zhang, L.; et al. Structure of the Sars-Cov-2 Spike Receptor-Binding Domain Bound to the Ace2 Receptor. *Nature* **2020**, *581*, 215–220.
- (26) Othman, H.; Bouslama, Z.; Brandenburg, J.-T.; da Rocha, J.; Hamdi, Y.; Ghedira, K.; Abid, N.-S.; Hazlehurst, S. Interaction of the Spike Protein Rbd from Sars-Cov-2 with Ace2: Similarity with Sars-Cov, Hot-Spot Analysis and Effect of the Receptor Polymorphism. *bioRxiv* **2020**, No. 2020.03.04.976027.
- (27) Zhang, G.; Pomplun, S.; Loftis, A. R.; Tan, X.; Loas, A.; Pentelute, B. L. Investigation of Ace2 N-Terminal Fragments Binding to Sars-Cov-2 Spike Rbd. *bioRxiv* **2020**, No. 2020.03.19.999318.
- (28) Basit, A.; Ali, T.; Rehman, S. U. Truncated Human Angiotensin Converting Enzyme 2; a Potential Inhibitor of Sars-Cov-2 Spike Glycoprotein and Potent Covid-19 Therapeutic Agent. *J. Biomol. Struct. Dyn.* **2020**, 1–10.
- (29) Panda, S. K.; Sen Gupta, P. S.; Biswal, S.; Ray, A. K.; Rana, M. K. Ace-2-Derived Biomimetic Peptides for the Inhibition of Spike Protein of Sars-Cov-2. *J. Proteome Res.* **2021**, *20*, 1296–1303.
- (30) Sithiyotha, T.; Chunsriviro, S. Computational Design of 25-Mer Peptide Binders of Sars-Cov-2. *J. Phys. Chem. B* **2020**, *124*, 10930–10942.
- (31) Chowdhury, S. M.; Talukder, S. A.; Khan, A. M.; Afrin, N.; Ali, M. A.; Islam, R.; Parves, R.; Al Mamun, A.; Sufian, M. A.; Hossain, M. N.; et al. Antiviral Peptides as Promising Therapeutics against Sars-Cov-2. *J. Phys. Chem. B* **2020**, *124*, 9785–9792.
- (32) Bhullar, K. S.; Drews, S. J.; Wu, J. Translating Bioactive Peptides for Covid-19 Therapy. *Eur. J. Pharmacol.* **2021**, *890*, No. 173661.
- (33) Du, Q.; Wang, S.; Wei, D.; Sirois, S.; Chou, K. C. Molecular Modeling and Chemical Modification for Finding Peptide Inhibitor against Severe Acute Respiratory Syndrome Coronavirus Main Proteinase. *Anal. Biochem.* **2005**, *337*, 262–270.
- (34) Ali, A. M.; Atmaj, J.; Van Oosterwijk, N.; Groves, M. R.; Dömling, A. Stapled Peptides Inhibitors: A New Window for Target Drug Discovery. *Comput. Struct. Biotechnol. J.* **2019**, *17*, 263–281.
- (35) Walensky, L. D.; Bird, G. H. Hydrocarbon-Stapled Peptides: Principles, Practice, and Progress. *J. Med. Chem.* **2014**, *57*, 6275–6288.
- (36) Moiola, M.; Memeo, M. G.; Quadrelli, P. Stapled Peptides-a Useful Improvement for Peptide-Based Drugs. *Molecules* **2019**, *24*, No. 3654.
- (37) Hillman, R. A.; Nadraws, J. W.; Bertucci, M. A. The Hydrocarbon Staple & Beyond: Recent Advances Towards Stapled Peptide Therapeutics That Target Protein-Protein Interactions. *Curr. Top. Med. Chem.* **2018**, *18*, 611–624.

- (38) Robertson, N. S.; Spring, D. R. Using Peptidomimetics and Constrained Peptides as Valuable Tools for Inhibiting Protein–Protein Interactions. *Molecules* **2018**, *23*, No. 959.
- (39) Walensky, L. D.; Kung, A. L.; Escher, I.; Malia, T. J.; Barbuto, S.; Wright, R. D.; Wagner, G.; Verdine, G. L.; Korsmeyer, S. J. Activation of Apoptosis in Vivo by a Hydrocarbon-Stapled Bh3 Helix. *Science* **2004**, *305*, 1466.
- (40) Curreli, F.; Victor, S. M. B.; Ahmed, S.; Drellich, A.; Tong, X.; Tseng, C.-T. K.; Hillyer, C. D.; Debnath, A. K. Stapled Peptides Based on Human Angiotensin-Converting Enzyme 2 (Ace2) Potently Inhibit Sars-Cov-2 Infection in Vitro. *mBio* **2020**, *11*, No. e02451-20.
- (41) Maas, M. N.; Hintzen, J. C. J.; Löffler, P. M. G.; Mecinović, J. Targeting Sars-Cov-2 Spike Protein by Stapled Hace2 Peptides. *Chem. Commun.* **2021**, *57*, 3283–3286.
- (42) Morgan, D. C.; Morris, C.; Mahindra, A.; Blair, C. M.; Tejeda, G.; Herbert, I.; Turnbull, M. L.; Lieber, G.; Willett, B. J.; Logan, N.; et al. Stapled Ace2 Peptidomimetics Designed to Target the Sars-Cov-2 Spike Protein Do Not Prevent Virus Internalization. *Pept. Sci.* **2021**, No. e24217.
- (43) Ford, N.; Vitoria, M.; Rangaraj, A.; Norris, S. L.; Calmy, A.; Doherty, M. Systematic Review of the Efficacy and Safety of Antiretroviral Drugs against Sars, Mers or Covid-19: Initial Assessment. *J. Int. AIDS Soc.* **2020**, *23*, No. e25489.
- (44) Mishra, S. K.; Tripathi, T. One Year Update on the Covid-19 Pandemic: Where Are We Now? *Acta Trop.* **2021**, *214*, No. 105778.
- (45) Bracken, C.; Gulyas, J.; Taylor, J. W.; Baum, J. Synthesis and Nuclear Magnetic Resonance Structure Determination of An.Alpha-Helical, Bicyclic, Lactam-Bridged Hexapeptide. *J. Am. Chem. Soc.* **1994**, *116*, 6431–6432.
- (46) Houston, M. E.; Campbell, A. P.; Lix, B.; Kay, C. M.; Sykes, B. D.; Hodges, R. S. Lactam Bridge Stabilization of A-Helices: The Role of Hydrophobicity in Controlling Dimeric Versus Monomeric A-Helices. *Biochemistry* **1996**, *35*, 10041–10050.
- (47) Osapay, G.; Taylor, J. W. Multicyclic Polypeptide Model Compounds. 1. Synthesis of a Tricyclic Amphiphilic.Alpha-Helical Peptide Using an Oxime Resin, Segment-Condensation Approach. *J. Am. Chem. Soc.* **1990**, *112*, 6046–6051.
- (48) Laverty, G.; McCloskey, A. P.; Gilmore, B. F.; Jones, D. S.; Zhou, J.; Xu, B. Ultrashort Cationic Naphthalene-Derived Self-Assembled Peptides as Antimicrobial Nanomaterials. *Biomacromolecules* **2014**, *15*, 3429–3439.
- (49) Blackwell, H. E.; Grubbs, R. H. Highly Efficient Synthesis of Covalently Cross-Linked Peptide Helices by Ring-Closing Metathesis. *Angew. Chem., Int. Ed.* **1998**, *37*, 3281–3284.
- (50) Zhou, W.; Xu, C.; Wang, P.; Luo, M.; Xu, Z.; Cheng, R.; Jin, X.; Guo, Y.; Xue, G.; Juan, L.; et al. N439k Variant in Spike Protein May Alter the Infection Efficiency and Antigenicity of Sars-Cov-2 Based on Molecular Dynamics Simulation. *bioRxiv* **2020**, No. 2020.11.21.392407.
- (51) Centers for Disease Control and Prevention. Sars-Cov-2 Variant Classifications and Definitions. <https://www.cdc.gov/coronavirus/2019-ncov/cases-updates/variant-surveillance/variant-info.html> (accessed May 19, 2021).
- (52) Deng, X.; Garcia-Knight, M. A.; Khalid, M. M.; Servellita, V.; Wang, C.; Morris, M. K.; Sotomayor-González, A.; Glasner, D. R.; Reyes, K. R.; Gliwa, A. S.; et al. Transmission, Infectivity, and Antibody Neutralization of an Emerging Sars-Cov-2 Variant in California Carrying a L452r Spike Protein Mutation. *medRxiv* **2021**, No. 2021.03.07.21252647.
- (53) Pettersen, E. F.; Goddard, T. D.; Huang, C. C.; Couch, G. S.; Greenblatt, D. M.; Meng, E. C.; Ferrin, T. E. Ucsf Chimera—a Visualization System for Exploratory Research and Analysis. *J. Comput. Chem.* **2004**, *25*, 1605–1612.
- (54) Shapovalov, M. V.; Dunbrack, R. L., Jr. A Smoothed Backbone-Dependent Rotamer Library for Proteins Derived from Adaptive Kernel Density Estimates and Regressions. *Structure* **2011**, *19*, 844–858.
- (55) Pierce, B. G.; Wiehe, K.; Hwang, H.; Kim, B. H.; Vreven, T.; Weng, Z. Zdock Server: Interactive Docking Prediction of Protein–Protein Complexes and Symmetric Multimers. *Bioinformatics* **2014**, *30*, 1771–1773.
- (56) Schneidman-Duhovny, D.; Inbar, Y.; Nussinov, R.; Wolfson, H. J. Patchdock and Symmdock: Servers for Rigid and Symmetric Docking. *Nucleic Acids Res.* **2005**, *33*, W363–W367.
- (57) Chen, R.; Li, L.; Weng, Z. Zdock: An Initial-Stage Protein–Docking Algorithm. *Proteins* **2003**, *52*, 80–87.
- (58) Mashiach, E.; Schneidman-Duhovny, D.; Peri, A.; Shavit, Y.; Nussinov, R.; Wolfson, H. J. An Integrated Suite of Fast Docking Algorithms. *Proteins* **2010**, *78*, 3197–3204.
- (59) Shang, J.; Ye, G.; Shi, K.; Wan, Y.; Luo, C.; Aihara, H.; Geng, Q.; Auerbach, A.; Li, F. Structural Basis of Receptor Recognition by Sars-Cov-2. *Nature* **2020**, *581*, 221–224.
- (60) Mashiach, E.; Nussinov, R.; Wolfson, H. J. Fiberdock: A Web Server for Flexible Induced-Fit Backbone Refinement in Molecular Docking. *Nucleic Acids Res.* **2010**, *38*, W457–W461.
- (61) Mashiach, E.; Nussinov, R.; Wolfson, H. J. Fiberdock: Flexible Induced-Fit Backbone Refinement in Molecular Docking. *Proteins* **2010**, *78*, 1503–1519.
- (62) D. E. Shaw Research. *Schrödinger Release 2020-4: Desmond Molecular Dynamics System. Maestro-Desmond Interoperability Tools*; Schrödinger: New York, NY, 2020.
- (63) Bowers, K. J.; Chow, E.; Xu, H.; Dror, R. O.; Eastwood, M. P.; Gregersen, B. A.; Klepeis, J. L.; Kolossvary, I.; Moraes, M. A.; Sacerdoti, F. D. et al. In *Scalable Algorithms for Molecular Dynamics Simulations on Commodity Clusters*, Proceedings of the 2006 ACM/IEEE Conference on Supercomputing; Association for Computing Machinery: Tampa, Florida, 2006.
- (64) Hoover, W. G. Canonical Dynamics: Equilibrium Phase-Space Distributions. *Phys. Rev. A* **1985**, *31*, 1695–1697.
- (65) Martyna, G. J.; Tobias, D. J.; Klein, M. L. Constant Pressure Molecular Dynamics Algorithms. *J. Chem. Phys.* **1994**, *101*, 4177–4189.
- (66) Harder, E.; Damm, W.; Maple, J.; Wu, C.; Reboul, M.; Xiang, J. Y.; Wang, L.; Lupyan, D.; Dahlgren, M. K.; Knight, J. L.; et al. Opls3: A Force Field Providing Broad Coverage of Drug-Like Small Molecules and Proteins. *J. Chem. Theory Comput.* **2016**, *12*, 281–296.
- (67) Holland Computer Center. <https://hcc.unl.edu/> (accessed Feb 14, 2021).
- (68) Jorgensen, W. L.; Maxwell, D. S.; Tirado-Rives, J. Development and Testing of the Opls All-Atom Force Field on Conformational Energetics and Properties of Organic Liquids. *J. Am. Chem. Soc.* **1996**, *118*, 11225–11236.
- (69) Schrödinger. Command-Line Only Scripts. <https://www.schrodinger.com/scriptcenter> (accessed Feb 14, 2021).
- (70) Kollman, P. A.; Massova, I.; Reyes, C.; Kuhn, B.; Huo, S.; Chong, L.; Lee, M.; Lee, T.; Duan, Y.; Wang, W.; et al. Calculating Structures and Free Energies of Complex Molecules: Combining Molecular Mechanics and Continuum Models. *Acc. Chem. Res.* **2000**, *33*, 889–897.
- (71) Li, J.; Abel, R.; Zhu, K.; Cao, Y.; Zhao, S.; Friesner, R. A. The Vsgb 2.0 Model: A Next Generation Energy Model for High Resolution Protein Structure Modeling. *Proteins* **2011**, *79*, 2794–2812.
- (72) Lensink, M. F.; Velankar, S.; Wodak, S. J. Modeling Protein–Protein and Protein–Peptide Complexes: Capri 6th Edition. *Proteins* **2017**, *85*, 359–377.
- (73) Wang, J.; Alekseenko, A.; Kozakov, D.; Miao, Y. Improved Modeling of Peptide–Protein Binding through Global Docking and Accelerated Molecular Dynamics Simulations. *Front. Mol. Biosci.* **2019**, *6*, No. 112.
- (74) Salmaso, V.; Sturlese, M.; Cuzzolin, A.; Moro, S. Exploring Protein–Peptide Recognition Pathways Using a Supervised Molecular Dynamics Approach. *Structure* **2017**, *25*, 655.e652–662.e652.
- (75) Schreiner, W.; Karch, R.; Knapp, B.; Ilieva, N. Relaxation Estimation of Rmsd in Molecular Dynamics Immunosimulations. *Comput. Math. Methods Med.* **2012**, *2012*, No. 173521.



(76) Schrödinger. Simulation Interactions Diagram. <https://www.schrodinger.com/newsletters/introducing-sid-simulation-interactions-diagram> (accessed Jan 15, 2021).

(77) Ghorbani, M.; Brooks, B. R.; Klauda, J. B. Critical Sequence Hotspots for Binding of Novel Coronavirus to Angiotensin Converter Enzyme as Evaluated by Molecular Simulations. *J. Phys. Chem. B* **2020**, *124*, 10034–10047.

(78) Jangra, S.; Ye, C.; Rathnasinghe, R.; Stadlbauer, D.; Alshammary, H.; Amoako, A. A.; Awawda, M. H.; Beach, K. F.; Bermúdez-González, M. C.; Chernet, R. L.; et al. Sars-Cov-2 Spike E484k Mutation Reduces Antibody Neutralisation. *Lancet Microbe* **2021**, DOI: 10.1016/S2666-5247(21)00068-9.

(79) Garcia-Beltran, W. F.; Lam, E. C.; St Denis, K.; Nitido, A. D.; Garcia, Z. H.; Hauser, B. M.; Feldman, J.; Pavlovic, M. N.; Gregory, D. J.; Poznansky, M. C.; et al. Multiple Sars-Cov-2 Variants Escape Neutralization by Vaccine-Induced Humoral Immunity. *Cell* **2021**, *184*, 2372.e2379–2383.e2379.

(80) Wang, P.; Casner, R. G.; Nair, M. S.; Wang, M.; Yu, J.; Cerutti, G.; Liu, L.; Kwong, P. D.; Huang, Y.; Shapiro, L.; et al. Increased Resistance of Sars-Cov-2 Variant P.1 to Antibody Neutralization. *bioRxiv* **2021**, No. 2021.03.01.433466.

(81) Tegally, H.; Wilkinson, E.; Giovanetti, M.; Iranzadeh, A.; Fonseca, V.; Giandhari, J.; Doolabh, D.; Pillay, S.; San, E. J.; Msomi, N.; et al. Emergence and Rapid Spread of a New Severe Acute Respiratory Syndrome-Related Coronavirus 2 (Sars-Cov-2) Lineage with Multiple Spike Mutations in South Africa. *medRxiv* **2020**, No. 2020.12.21.20248640.

(82) Centers for Disease Control and Prevention. Science Brief: Emerging Sars-Cov-2 Variants. <https://www.cdc.gov/coronavirus/2019-ncov/more/science-and-research/scientific-brief-emerging-variants.html> (accessed May 19, 2021).

(83) Vasques Nonaka, C. K.; Franco, M. M.; Gräf, T.; Almeida Mendes, A. V.; Santana de Aguiar, R.; Giovanetti, M.; Solano de Freitas Souza, B. Genomic Evidence of a Sars-Cov-2 Reinfection Case with E484k Spike Mutation in Brazil. **2021**, 202101.0132.v2. <https://www.preprints.org/manuscript/202101.0132/v2>.

(84) Davies, N. G.; Abbott, S.; Barnard, R. C.; Jarvis, C. I.; Kucharski, A. J.; Munday, J. D.; Pearson, C. A. B.; Russell, T. W.; Tully, D. C.; Washburne, A. D.; et al. Estimated Transmissibility and Impact of Sars-Cov-2 Lineage B.1.1.7 in England. *Science* **2021**, *372*, No. eabg3055.

(85) Wiehe, K.; Peterson, M. W.; Pierce, B.; Mintseris, J.; Weng, Z. Protein-Protein Docking: Overview and Performance Analysis. *Methods Mol. Biol.* **2008**, *413*, 283–314.

(86) Weng, G.; Wang, E.; Chen, F.; Sun, H.; Wang, Z.; Hou, T. Assessing the Performance of Mm/Pbsa and Mm/Gbsa Methods. 9. Prediction Reliability of Binding Affinities and Binding Poses for Protein-Peptide Complexes. *Phys. Chem. Chem. Phys.* **2019**, *21*, 10135–10145.

(87) Hou, T.; Wang, J.; Li, Y.; Wang, W. Assessing the Performance of the Molecular Mechanics/Poisson Boltzmann Surface Area and Molecular Mechanics/Generalized Born Surface Area Methods. II. The Accuracy of Ranking Poses Generated from Docking. *J. Comput. Chem.* **2011**, *32*, 866–877.